The Late-Stage Steps of *Burkholderia cenocepacia* Protein O-Linked Glycan Biosynthesis Are Conditionally Essential.

Leila Jebeli[1], Taylor A. McDaniels[1], Duncan T. T. Ho[1], Hamza Tahir[1], Nicholas L. Kai-Ming[1], Molli Mcgaw[1], Kristian I. Karlic[1], Jessica M. Lewis[2] and Nichollas E. Scott[1]

[1]Department of Microbiology and Immunology, University of Melbourne at the Peter Doherty Institute for Infection and Immunity, Melbourne 3000, Australia

Current addresses:

[2]School of Life Sciences, University of Warwick, Coventry, CV4 7AL, UK.

[#]To whom correspondence and requests for materials should be addressed N.E.S (Nichollas.scott@unimelb.edu.au)

Key words: Glycosylation, *Burkholderia cenocepacia*, *Burkholderia*, Post-translational modifications, Proteomics, Glycoproteomics

Abstract:

Periplasmic *O*-linked protein glycosylation is a highly conserved process observed across the *Burkholderia* genus. Within Burkholderia, protein glycosylation requires the five gene cluster known as the *O*-glycosylation cluster (OGC, *ogcXABEI*) which facilitates the construction of the *O*-linked trisaccharide attached to periplasmic proteins. Previous studies have reported conflicting results regarding the essentiality of *ogcA* and *ogcX*, predicted to be involved in the last steps in *O*-linked glycan biosynthesis. Within this work, we aimed to dissect the impact of the loss of *ogcA* and *ogcX* on *Burkholderia cenocepacia* viability. We demonstrate that the loss of *ogcA* or *ogcX* appears detrimental if glycosylation is initiated leading to marked phenotypic effects. Proteomic analysis supports that the loss of *ogcA*/*ogcX* both blocks glycosylation and drives pleotropic effects in the membrane proteome, resulting in the loss of membrane integrity. Consistent with this, strains lacking *ogcA* and *ogcX* exhibit increased sensitivity to membrane stressors including antibiotics and demonstrate marked changes in membrane permeability. These effects are consistent with fouling of the undecaprenyl pool due to dead-end *O*-linked glycan intermediates, and consistent with this, we show that modulation of the undecaprenyl pool through the overexpression of undecaprenyl pyrophosphate synthase (UppS) as well as early-stage OGC biosynthesis genes (*ogcI* and *ogcB*) impacts *B. cenocepacia* viability. These findings demonstrate disrupting *O*-linked glycan biosynthesis or transport appears to dramatically impact *B. cenocepacia* viability, supporting the assignment of *ogcA* and *ogcX* as conditionally essential.

Importance:

Protein glycosylation, a conserved process in Burkholderia species, utilizes glycans generated by the O-glycosylation cluster (OGC), which is composed of five genes (*ogcX, ogcA*, *ogcB*, *ogcE*, and *ogcI*). In this study, we demonstrate that the loss of ogcA or ogcX significantly affects the physiology of *Burkholderia cenocepacia*. Using complementary genetic approaches and proteomic techniques, we show that the loss of ogcA or ogcX blocks glycosylation, alters the cell membrane, and sensitizes cells to stressors such as antibiotics. This increased sensitivity to membrane stress is caused by the accumulation of dead-end O-linked glycan intermediates, which sequester the limited and essential undecaprenyl pool within *B. cenocepacia*. These findings highlight that *ogcA* and *ogcX* are conditionally essential for *B. cenocepacia* survival and provides mechanistic insight into how protein glycosylation fidelity—the use of specific glycans for protein glycosylation—is controlled in *Burkholderia* species.

Introduction:

Across bacterial species many surface polysaccharides are synthesized utilising the essential polyisoprenoid lipid undecaprenyl phosphate (Und-P) [1,2]. Functioning as a chemical carrier, Und-P provides an assembly point for the stepwise construction of diverse lipid-linked oligosaccharide units at the inner face of the cytoplasmic membrane within Gram-negative and Gram-positive species [1,2]. By providing a tethering point to enable glycan elongation, Und-P allows the construction of a range of glycans, which upon translocation into the periplasmic space can be integrated into glycoconjugates including peptidoglycan, O-antigens, capsules, and exopolysaccharides [3,4]. While Und-P and its phosphorylated form undecaprenyl pyrophosphate (Und-PP) are important for the construction of surface carbohydrates, these molecules account for less than 1% of the total lipid pool [5], resulting in competition for available Und-P and the need for rapid flux of oligosaccharide units through the Und-P/Und-PP cycle [6,7]. Under normal physiological conditions, *de novo* synthesis and recycling of Und-P/Und-PP are able to meet physiological demands [6,7], yet it is recognised that genetic manipulations that result in Und-PP-glycan intermediates that sequester the Und-P/Und-PP pool can dramatically impact cellular viability, morphology and growth [6-11]. Understanding Und-PP-glycan intermediates with the capacity to foul the Und-P/Und-PP pool has the potential to not only aid antimicrobial development [12,13] but also explain the mechanisms underpinning the homogeneity observed within the glycan structures of glycoconjugates [14-16].

Ensuring only glycans possessing specific structural configurations, herein referred to as glycan fidelity, can translocate into the periplasmic space ensures homogeneity within oligosaccharide units constructed utilising the Und-P/Und-PP pool [3,4]. For many glycoconjugates generated using Und-PP linked oligosaccharides, the addition of specific glycan components is a pre-requisite for effective translocation across the cytoplasmic membrane by the actions of dedicated translocases known as flippases [17-19]. Of the known flippases the Wzx enzymes represent a highly diverse family of enzymes [19,20] responsible for the translocation of a range of carbohydrates including O-antigens [21], capsules [22,23], exopolysaccharides [24], and the enterobacterial common antigen (ECA) [10]. While Wzx flippases were initially thought to possess limited capacity for the recognition of glycan structures [25,26], it has increasingly become clear multiple features of their cognate glycans beyond the

initiating sugar influence translocation efficiency when Wzx enzymes are expressed under native-like conditions [3,15,27]. This specificity results in discrete Wzx flippases being observed genetically linked to their cognate glycan clusters [15,22,23,27] with Wzx enzymes suggested to function as quality control mechanisms [16], ensuring only "complete" glycans are effectively translocated to the periplasmic space. The specificity for complete glycans by Wzx flippases in concert with the extension of glycans beyond key points committing Und-PP-linked oligosaccharides to the generation of specific glycans [11,25,28-31] leads to Und-PP-linked intermediates, if unable to be completed, driving detrimental phenotypes [6,7,11]. These deleterious phenotypes, which are attributed to the sequestration of the Und-P/Und-PP pool [6,7,11], can rapidly lead to the emergence of suppressor mutations, which complicates the analysis of Und-P/Und-PP glycan biosynthesis pathways by obfuscating the role of specific glycan biosynthesis genes [9,32,33]. While these potential confounding effects are now well appreciated for the O-antigens [6,11], capsule [34] and ECA [7], this phenomenon has not been explored within glycans used for other glycoconjugates such as protein glycosylation.

Protein glycosylation is widespread across bacterial species [35,36] including members of the *Campylobacter* [37,38], *Neisseria* [39-43], and *Burkholderia* [44-46] genera. To date, several Und-P/Und-PP dependent glycosylation systems have been described, which utilise the Und-P lipid pool to enable periplasmic glycosylation leading to glycosylation of tens to hundreds of proteins [36,47-49]. While similarities within the biosynthetic clusters used for protein glycosylation systems and lipooligosaccharide biosynthetic clusters have been previously highlighted [35,36], a notable difference within well-characterised glycosylation systems is the use of ABC transporter-based flippases [35,36] as opposed to Wzx flippases. These ABC transporter-based flippases, such as PglK (also known as WlaB[50]) within *Campylobacter* sp. [51,52] and PglF within *Neisseria* sp. [53-55] are dispensable for glycosylation [52,55] as well as possess relaxed glycan specificities as demonstrated using heterogenous expression studies for PglK [52] and the observation of glycan microheterogeneity within *Neisseria* [56,57]. The tolerance of these glycosylation pathways to both glycan alterations, as well as the loss of their flippases, is in stark contrast to the strict specificity and essentiality seen within other Und-P/Und-PP dependent systems, yet not all Und-P/Und-PP dependent protein glycosylation systems possess ABC transporter flippases.

Within *Burkholderia* species, periplasmic glycosylation is highly conserved [44-46], leading to nearly exclusive modification of serine residues [44] with a trisaccharide corresponding to β-Gal-(1,3)–α-GalNAc-(1,3)–β-GalNAc [46]. *Burkholderia O*-linked glycan assembly is mediated by a single gene cluster known as the *O*-linked Glycosylation Cluster (*OGC*) consisting of five genes (*ogcX*, *A*, *B*, *E* and *I* corresponding to BCAL3114 to BCAL3118 within *Burkholderia cenocepacia* respectively) [46]. Our current model of glycan assembly (**Figure 1A**) supports OgcE (BCAL3117) as a UDP-Glc / UDP-GlcNAc epimerase, OgcI (BCAL3118) as the initiating glycotransferase for the *O*-linked glycan, OgcB (BCAL3116) and OgcA (BCAL3115) work as extending glycosyltransferases responsible for the addition of the second GalNAc and final Gal residues respectively, and the putative Wzx flippase OgcX (BCAL3114), responsible for the translocation of the glycan across the inner membrane [46] where it can then be transferred to glycoproteins by the oligosaccharyltransferase PglL (BCAL0960) [46,58]. Previous studies have provided experimental evidence for the function of OgcB, OgcE and OgcI [46] yet contradictory results have been obtained for the enzymes OgcA and OgcX. While it has been noted that despite multiple attempts an *ogcA* knockout has been unable to be generated [46], the loss of *ogcX* has been previously reported to be tolerated within *B. cenocepacia* [46]. Similarly, saturation transposon studies from several *Burkholderia* species [59-61] have revealed variability in the ability to disrupt *ogcA* and *ogcX,* with some studies concluding these enzymes are essential [61] while others suggest that at least for *ogcA* disruptions within this gene may be tolerated [60]. These observations support that unlike the glycosylation systems of the *Campylobacter* and *Neisseria* genera, disruptions in glycan biosynthesis steps may not be tolerated within *Burkholderia.* These contradictory results support further assessments are required to dissect the impact of loss of *ogcA* and *ogcX* on viability and protein glycosylation.

Within this work, we sought to assess the requirement of *ogcA* and *ogcX* for protein glycosylation and the impact of the loss of these *ogc* components on *B. cenocepacia.* Utilising complementary genetic approaches, including *ogc* complementation within strains lacking the *ogc* cluster [46,62] as well as glycosylation inducible strains containing the initiating transferase, *ogcI,* under rhamnose control [63], we assess the proteomic and physiological impacts of the loss of *ogcA* and *ogcX.* We demonstrate that in the absence of glycosylation initiation, *ogcA* and *ogcX* are dispensable, yet upon glycosylation initiation, loss of these genes leads to growth defects, widespread proteomic impacts, changes in the membrane integrity

and the absence of observable glycosylation. While these changes can be complemented or partially compensated by the modulation of enzymes associated with *de novo* synthesis of Und-P, we also observe that modulation of early steps in the *O*-linked glycan biosynthesis pathways can also lead to loss of viability. This data supports that the construction of the *O*-linked glycan in *B. cenocepacia* is finely tuned, and modulation or blocking of steps impacts viability. Thus, akin to other Und-P/Und-PP dependent systems, which utilise Wzx flippases, the loss of either *ogcA* or *ogcX* is conditionally detrimental upon glycosylation initiation.

Methods:

Bacterial strains and growth conditions: Bacterial strains used in this study are listed in **Supplementary Table 1**. Strains were cultured in Lysogeny Broth (LB) or on LB agar (1.5–2% w/v), prepared in accordance with the manufacturer's instructions containing 0.5% NaCl (BD™, New Jersey, USA). Liquid cultures were incubated overnight at 37°C with shaking, while agar plates were incubated at 37°C overnight for *Escherichia coli* and 24–72 hours for *B. cenocepacia*. When required, LB was supplemented with 200 µg/mL diaminopimelic acid (DAP; Sigma) to support growth of *E. coli* RHO3 [64]. Antibiotics were added to cultures to select or maintain plasmids/ transconjugants at a final concentration of 50 µg/mL trimethoprim for *E. coli* and 100 µg/mL for *B. cenocepacia*, 20 µg/mL tetracycline for *E. coli* and 150 µg/mL for *B. cenocepacia* and 50 µg/mL kanamycin for *E. coli*. To counter-select helper and donor *E. coli* strains in triparental and quadparental mating, ampicillin at 100 µg/mL and polymyxin B at 25 µg/mL were added [65]. Culturing of strains containing the temperature-sensitive plasmid pFlptet (see **Supplementary Table 2**) was undertaken at 30°C with cultures shifted to 37°C to enable plasmid curing [66]. Curing of pDAI-SceI-SacB was achieved by sucrose counterselection [65]. Induction of *B. cenocepacia* strains was performed by either adding 20% filter-sterilised L-rhamnose monohydrate (Sigma) or 1 mM 4-Isopropylbenzoic acid (cumate, Sigma) to LB broth or LB agar at a concentration of 0.05%-1% for rhamnose and 100 µM for cumate. For non-induced controls, an equivalent volume of solvent (sterile water for rhamnose and ethanol for cumate) was added to the culture media.

Recombinant DNA methods: Oligonucleotides used in this study are listed in **Supplementary Table 3**, with all PCR amplifications for cloning carried out using Q5 DNA polymerase (New England Biolabs) with the addition of 2% DMSO for the amplification of *B. cenocepacia* DNA, due to its high GC content. Genomic DNA isolations were performed using an EZ-10 Spin Column Bacterial Genomic DNA Mini-Preps Kit (Bio Basic), while PCR clean up and restriction digest purifications were performed with a Zymoclean Gel DNA Recovery Kit (ZymoResearch). pGPI-SceI [67] mutagenesis plasmids were constructed using Gibson assembly [68] with DNA fragments flanking genes of interest amplified by Q5-based PCR. *Sma*I-linearized pGPI-SceI and Q5-amplified fragments were assembled using the NEBuilder® HiFi DNA master mix

according to the manufacturer's instructions (New England Biolabs). pSCrhaB2 [63] and pMLBAD [69] based expression vectors containing genes of interest were generated using Gibson Assembly or restriction endonuclease-based cloning. For Gibson Assembly, PCR-amplified fragments were introduced into *Nde*I/*Xba*I-linearized pSCrhaB2 or PCR-derived pMLBAD vector backbones using the NEBuilder® HiFi DNA master mix. For restriction endonuclease-based cloning, PCR-amplified fragments were digested with *Nde*I/*Xba*I and then ligated into *Nde*I/*Xba*I-linearized pSCrhaB2 overnight at 16°C using T4 Ligase (New England Biolabs). Modification of pSCrhaB2 to remove *ogc*A, *ogc*B, *ogc*I and *ogc*X was achieved by assembling PCR-amplified fragments into *Nde*I/*Hind*III-linearized pSCrhaB2 using the NEBuilder® HiFi DNA master mix.

Prior to Gibson Assembly and restriction cloning all DNA fragments were assessed for correctness based on size using agarose gel electrophoresis. Ligated/assembled plasmid mixtures were introduced into chemically competent *E. coli* PIR2 cells via heat shock transformation [70], plated on selective media and screened using colony PCR with GoTaq® Green Master Mix (Promega). All plasmids used in this study have been confirmed by either Sanger sequencing using the Australian Genome Research Facility (Melbourne, Australia) or nanopore plasmid sequencing using Plasmidsaurus (SNPsaurus LLC, Eugene, OR). Donor plasmids for biparental and quadparental mating were further isolated and introduced into *E. coli* RHO3 [64] via electroporation [70] to improve conjugation efficiency into *B. cenocepacia*. A complete list of the plasmids used in this study, along with a summary of their construction, is provided in **Supplementary Table 2**.

Conjugation of plasmids into *B. cenocepacia*: Plasmids were introduced into *B. cenocepacia* K56-2 via one of three approaches: I) biparental mating using the conjugative diaminopimelic acid auxotroph *E. coli* RHO3 [64] for the introduction of pFLPtet or pDAI-SceI-SacB; II) triparental mating [65] using *E. coli* PIR2 containing pRK2013 (helper plasmid) [71] and *E. coli* PIR2 carrying pGPI-SceI-derived vectors or pSCrhaB2/pMLBAD expression vectors (donor plasmid); or III) quadparental mating using *E. coli* PIR2 containing pRK2013 [71], *E. coli* PIR2 containing pTNS3 (Tn7 transposase plasmid) [72] and *E. coli* RHO3 carrying pUC18T-mini-Tn7T-Tp-rha-ogcI (donor plasmid) for the chromosomal integration of miniTn7-rha-ogcI. Conjugations were allowed to

proceed for 24 hours, then successful transconjugants were selected with trimethoprim, and the introduction of plasmids of interest confirmed using PCR-based screening. For the generation of unmarked, non-polar deletions using pGPI-SceI and the removal of the trimethoprim resistance marker within the integrated miniTn7, additional rounds of conjugation were undertaken to introduce pDAI-SceI-SacB [67,73] or pFLPtet[66] respectively using tetracycline based selection. pGPI-SceI/pDAI-SceI-SacB-based mutagenesis as well as FLP-based removal of the trimethoprim resistance marker within Tn7 were confirmed using screening oligonucleotides (**Supplementary Table 3**) by colony PCR using GoTaq® Green Master Mix. Numeration of transconjugants derived from the introduction of pSCrhaB2-*ogc* and its derivatives into *B. cenocepacia* wildtype (WT) or *B. cenocepacia* Δ*ogc* were assessed across three independent conjugations.

Spot plate assays: Colony morphology and membrane stress tolerance assessments were performed as previously described [74-76] using spot plate assays. For spot plate assays, strains of interest were grown overnight in LB broth without induction, normalised to an OD_{600} of 1.0 and then serially diluted from 10^{-1} to 10^{-6}. 10 µL of diluted cultures were manually spotted onto LB plates with and without inducers (1% Rhamnose /100 µM cumate). 0.01% SDS or 2% NaCl were added to plates to assess membrane integrity and the impact of osmotic stress on viability with and without inducers. For assays of *B. cenocepacia* strains containing pSCrhaB2- or pMLBAD-based expression vectors, trimethoprim was added to plates to ensure the maintenance of plasmids. For antimicrobial resistance, spot assays concentrations corresponding to at or below the broth dilution defined MIC assays (**Supplementary Figure 10**) were used for trimethoprim (8 µg/mL), tetracycline (16 µg/mL), chlorhexidine (4 µg/mL), ceftazidime (4 µg/mL), and rifampicin (32 µg/mL) on cation-adjusted Mueller–Hinton agar. Spots were allowed to dry, and plates were incubated for 48 hours at 37°C before being imaged. All spot assays were assessed using at least three independent replicates. Colony area measurements were undertaken using Fiji [77], assessing the size of 20 colonies per spot assay with three independent assays conducted with t-tests used to determine significant changes in colony size as well as viable counts between induced and non-induced conditions.

Plate-based viability and growth kinetics assays. To assess viability and growth kinetics, 96-well-based growth assays were undertaken as previously described [62]. Bacterial strains were grown overnight in LB, normalised to an OD_{600} of 1.0 and diluted 1 in 100 with LB supplemented with or without combinations of inducers and/or membrane stressors (0.01% SDS or 2% NaCl). 200 µL of diluted cultures were added to 96-well flat-bottom plates and incubated at 37°C with shaking at 200 rpm in a CLARIOstar plate reader (BMG LABTECH, Inc.), measuring the optical density at 600 nm every 10 minutes over 24 hours. Growth assays were assessed in at least technical triplicate across three independent biological replicates.

Fluorescence Detection of the permeability of inner and outer membranes: Permeability of the inner membrane was assessed using Hoechst 33342 (Abcam) as previously described [78-80]. Briefly, bacterial strains were grown overnight in LB (with and without 1% Rhamnose), normalised to an OD_{600} of 2.0, washed three times with PBS and dispensed at 100 µL aliquots into 96-well black clear-bottomed plates. 100 µL of PBS and heat-killed bacteria were added to the plates as controls. 100 µL of 2.5 µM Hoechst 33342 in PBS was added to wells to generate bacterial suspensions with an OD_{600} of 1.0 and a final concentration of 1.25 µM Hoechst 33342. Fluorescence was measured in a CLARIOstar plate reader using an excitation of 361nm and emission detection at 486nm. The fluorescence intensity was first normalised by assigning the value of 100 to the heat-killed and 0 to the non-induced parental strain. To assess outer membrane permeability, 1-*N*-phenylnaphthylamine (NPN, Thermo Fisher Scientific) was used as described previously [81-83]. Cultures were normalised as above, washed three times with 5 mM HEPES, pH 7.4, 10 mM sodium azide and dispensed at 100 µL aliquots into 96-well black clear-bottomed plates. 100 µL of 5 mM HEPES, pH 7.4, 10 mM sodium azide was added to the plates as a blank. 100 µL of 20 µM NPN in 5 mM HEPES, pH 7.4, 10 mM sodium azide was added to wells to generate bacterial suspensions with an OD_{600} of 1.0 and a final concentration of 100 µM NPN. Fluorescence was measured in a CLARIOstar plate reader using an excitation of 350nm and emission detection at 420nm. The fluorescence intensity was first normalised by assigning the value of 0 to the non-induced parental strain. Hoechst 33342 and NPN assays were assessed in technical triplicate across five independent biological replicates. To assess viability and comparable cell numbers, the OD-adjusted bacterial suspensions were serially diluted and plated on LB and viable cells numerated

(**Supplementary Figure 8**). The fluorescence intensity from both assays was normalised against the determined cell number.

Preparation of proteomic samples: *B. cenocepacia* cultures for proteomic analysis were grown overnight with or without induction with rhamnose or cumate as outlined above with shaking at 180 rpm. Overnight cultures were normalised to an OD_{600} of 1.0 and then collected by centrifugation at 10,000 x *g* at 4˚C for 10 minutes, washed 3 times with ice-cold PBS and then snap frozen at -80˚C until processing. Frozen whole cell samples were prepared for analysis using sodium deoxycholate (SDC) based lysis and the in-StageTip preparation approach as previously described [84]. OgcX complementation assays were undertaken using SDS-based lysis and S-trap sample preparation to improve the detection of OgcX. For in-StageTip preparation, cells were resuspended in 4% sodium deoxycholate (SDC), 100 mM Tris pH 8.0 and boiled at 95˚C with shaking (2000 rpm) for 10 minutes to solubilise the proteome. Samples were allowed to cool for 10 minutes and then boiled for a further 10 minutes (95°C, 2000 rpm) before the protein concentrations were determined by bicinchoninic acid assays (Thermo Fisher Scientific). Samples were reduced/alkylated with the addition of Tris-2-carboxyethyl phosphine and chloroacetamide (final concentration 10 mM and 40 mM, respectively), and samples were incubated in the dark for 0.5-1 hour at 45˚C. Following reduction/alkylation, samples were digested overnight with Trypsin (1/50 w/w Solu-trypsin, Sigma) at 37˚C with shaking at 1000rpm. Digests were then quenched with the addition of 1.25 volumes of isopropanol before being cleaned up using SDB-RPS (Sigma) StageTips.

For S-trap-based preparation, cells were resuspended in 4% sodium dodecyl sulphate (SDS), 100 mM Tris pH 8.0, and boiled at 95˚C with shaking (2000 rpm) for 10 minutes; the protein concentrations were then determined by bicinchoninic acid assays, and samples were reduced/alkylated as above. Samples were acidified to 1.2% phosphoric acid and diluted with seven volumes of S-trap wash buffer (90% methanol, 100mM tetraethylammonium bromide pH 7.1) before being loaded onto S-traps mini spin columns (Protifi) and washed 3 times with 400 µL of S-trap wash buffer. Samples were then digested with 2 µg of Trypsin (a 1:50 protease/protein ratio) in 100 mM tetraethylammonium bromide (TEAB) overnight at 37 °C before being collected by centrifugation with washes of 100 mM TEAB, followed by 0.2%

formic acid followed by 0.2% formic acid / 50% acetonitrile before being dried by vacuum centrifugation at room temperature and stored at -20˚C.

SDB-RPS StageTips-based clean-up of digests was undertaken by adjusting or resuspending samples in 50% isopropanol, 1% trifluoroacetic acid and then loading them on in-house created SDB-RPS StageTips, which were prepared according to previously described protocols [84-86]. Briefly, five frits of SDB-RPS were excised using a blunt 16-gauge Hamilton needle and loaded into 200 µL tips. SDB-RPS StageTips were placed in a Spin96 tip holder [85] to enable batch-based spinning of samples and tips conditioned with 100% acetonitrile, followed by 30% methanol, 1% trifluoroacetic acid, followed by 90% isopropanol, 1% trifluoroacetic acid with each wash spun through the column at 1000 x *g* for 3 minutes. Acidified isopropanol/peptide mixtures were loaded onto the SDB-RPS columns and spun through tips before being washed with 90% isopropanol, 1% trifluoroacetic acid, followed by 90% ethyl acetate, 1% trifluoroacetic acid, followed by 1% trifluoroacetic acid in Milli-Q water. Peptide samples were eluted with 80% acetonitrile, 5% ammonium hydroxide and dried by vacuum centrifugation at room temperature and stored at -20˚C.

LC-MS analysis of DDA samples. Cleaned-up peptide samples were re-suspended in Buffer A* (2% acetonitrile, 0.1% trifluoroacetic acid in Milli-Q water) and separated using a two-column chromatography set-up on a Dionex Ultimate 3000 UPLC composed of a PepMap100 C18 20 mm x 75 µm trap and a PepMap C18 500 mm x 75 µm analytical column (Thermo Fisher Scientific) coupled to a Orbitrap Fusion™ Lumos™ Tribrid™ Mass Spectrometer (Thermo Fisher Scientific) with datasets collected with and without the use of the FAIMS Pro interface (Thermo Fisher Scientific). 145-minute gradients were run for each sample, with samples loaded onto the trap column with 98% Buffer A (2% acetonitrile, 0.1% formic acid in Milli-Q water) and 2% Buffer B (80% acetonitrile, 0.1% formic acid) with peptides separated by altering the buffer composition from 2% Buffer B to 28% B over 126 minutes, then from 28% B to 40% B over 9 minutes, then from 40% B to 80% B over 3 minutes, the composition was held at 80% B for 2 minutes, and then dropped to 2% B over 2 minutes and held at 2% B for another 3 minutes. For datasets collected without the use of the FAIMS Pro interface, the Lumos™ Mass Spectrometer was operated in a data-dependent mode, switching between the

collection of a single Orbitrap MS scan (450-2000 m/z, maximal injection time of 50 ms, an AGC of maximum of $4*10^5$ ions and a resolution of 60k) acquired every 3 seconds followed by Orbitrap MS/MS HCD scans of precursors (NCE 30%, maximal injection time of 80 ms, an AGC set to a maximum of $1.25*10^5$ ions and a resolution of 30k). For datasets collected with the FAIMS Pro interface, a data-dependent stepped FAIMS approach was utilised with three different FAIMS CVs -25, -45 and -65, as previously described [87]. For each FAIMS CV a single Orbitrap MS scan (450-2000 m/z, maximal injection time of 50 ms, an AGC of maximum of $4*10^5$ ions and a resolution of 60k) was acquired every 1.2 seconds followed by Orbitrap MS/MS HCD scans of precursors (NCE 30%, maximal injection time of 80 ms, an AGC set to a maximum of $1.25*10^5$ ions and a resolution of 30k). HCD scans containing HexNAc-associated oxonium ions (204.0867, 138.0545 and 366.1396 m/z) triggered two additional product-dependent MS/MS scans [88] of potential glycopeptides; an Orbitrap EThcD scan (NCE 15%, maximal injection time of 150 ms, AGC set to a maximum of $2*10^5$ ions with a resolution of 30k using the extended mass range setting to improve the detection of high mass glycopeptide fragment ions [89]) and a stepped collision energy HCD scan (using NCE 35% with 5% Stepping, maximal injection time of 150 ms, an AGC set to a maximum of $2*10^5$ ions and a resolution of 30k).

LC-MS analysis of DIA samples: Cleaned-up peptide samples were resuspended in Buffer A* and separated using a two-column chromatography set-up on a Dionex Ultimate 3000 UPLC composed of a PepMap100 C18 20 mm x 75 µm trap and a PepMap C18 500 mm x 75 µm analytical column. Samples were concentrated onto the trap column at 5 µL/min for 5 minutes with 98% Buffer A and 2% Buffer B, then infused into an Orbitrap Fusion™ Lumos™ Tribrid™ Mass Spectrometer at 300 nL/minute via the analytical column. 125-minute analytical runs were undertaken by altering the buffer composition from 3% Buffer B to 25% B over 112 minutes, then from 25% B to 40% B over 4 minutes, then from 40% B to 80% B over 1 minute. The composition was held at 80% B for 3 minutes, and then dropped to 3% B over 1 minute before being held at 3% B for another 4 minutes. Data was collected in a Data-independent manner with a single MS1 event (120k resolution, AGC $1*10^6$, 350-1400 m/z) and 50 MS2 scans (NCE 30%, 30k resolution, AGC $1*10^6$, 200-2000 m/z and a maximal

injection time of 55 ms) of a width of 13.7 m/z collected over the mass range of 360 to 1033.5 m/z.

DDA-based proteomic analysis: DDA datasets were analysed using MSFragger (versions 18.0, 19.0, 20.0 or 22.0) [90-92]. Samples were searched with a Tryptic specificity, allowing a maximum of two missed cleavage events and Carbamidomethyl set as a fixed modification of Cysteine while oxidation of Methionine allowed as a variable modification. The *Burkholderia* glycans $HexHexNAc_2$ (elemental composition: $C_{22}O_{15}H_{36}N_2$, mass: 568.2115 Da) and Suc-$HexHexNAc_2$ (elemental composition: $C_{26}O_{18}H_{40}N_2$, mass: 668.2276 Da) were included as variable modifications at Serine in line with the strong preference for PglL glycosylation at Serine residues [44]. The glycan fragment ions were defined as 204.0866, 186.0760 168.0655, 366.1395, 144.0656, 138.0550, 466.1555 and 407.1594. A maximum mass precursor tolerance of 20 ppm was allowed at both the MS1 and MS2 levels. Samples were searched against the *B. cenocepacia* reference proteome J2315 (Uniprot accession: UP000001035, 6,993 proteins, downloaded July 24th 2020) [93] supplemented with the proteins RhaS (HTH-type transcriptional activator RhaS, P09377), RhaR (HTH-type transcriptional activator RhaR, P09378), TmpR (Dihydrofolate reductase resistance marker, P00384) and CymR (HTH-type transcriptional regulator CymR, O33453). MS1-based quantitation was undertaken using MaxLFQ [94] with matching between runs enabled. Statistical analysis of protein abundances was undertaken using Perseus [95] with missing values imputed based on the total observed protein intensities with a range of 0.3 σ and a downshift of 2.5 σ. Biological replicates were grouped together, and student t-tests were used to compare individual groups with a minimum fold change of +/- 1 considered for further analysis. Data visualization was undertaken using ggplot2 [96] in R.

DIA-based proteomic analysis: DIA Datasets were searched using DIA-library free analysis within Spectronaut (version 17.6). Data files were searched against the *B. cenocepacia* K56-2 proteome (Uniprot accession: UP000011196, 7467 proteins, downloaded October 13th 2020) [97] and *B. cenocepacia* strain J2315 (Uniprot accession: UP000001035) [93], merging these proteomes enabling the matching of proteins to both J2315 and K56-2 accessions. Oxidation

of Methionine was allowed as a variable modification, Carbamidomethyl was set as a fixed modification of Cysteine, and protease specificity was set to trypsin. Protein quantitation was undertaken using MaxLFQ [94] based analysis. The precursor PEP was altered to 0.01 from the default 0.2 to improve quantitative accuracy, with all single peptide protein matches excluded. Statistical analysis was undertaken using Perseus [95] with missing values imputed based on the total observed protein intensities with a range of 0.3 σ and a downshift of 2.5 σ. Biological replicates were grouped together, and student t-tests were used to compare individual groups with a minimum fold change of +/- 1 considered for further analysis. Multiple hypothesis correction was undertaken using a permutation-based FDR approach allowing an FDR of 5%. Enrichment analysis using Fisher exact tests was undertaken in Perseus using Gene Ontology (GO) terms obtained from Uniprot (*B. cenocepacia* strain J2315 proteome: UP000001035). Data visualization was undertaken using ggplot2 [96] in R.

Data availability: All mass spectrometry data (RAW files, FragPipe outputs, Spectronaut outputs / experiment files, Rmarkdown scripts, and output tables) have been deposited into the PRIDE ProteomeXchange repository [98,99]. All PRIDE accession numbers, descriptions of the associated experiments and experiment types (DIA or DDA) are provided in **Supplementary Table 4**. All proteomics data tables have been deposited in Figshare and are accessible by the link: https://figshare.com/s/da1cee5ddc955ef29afe.

Results:

Loss of *ogcA* and *ogcX* impacts viability of *B. cenocepacia*

To dissect the impact of individual *ogc* genes on viability, we established a rhamnose-inducible vector pSCrhaB2 [63] containing the *ogc* cluster (pSCrhaB2-*ogc*) herein referred to as p*ogc* (**Figure 1B**), and assessed its ability to restore glycosylation within *B. cenocepacia* Δ*ogc* [46]. Using mass spectrometry-based proteomics, we confirmed the restoration of glycosylation regardless of rhamnose induction and the absence of glycosylation within Δ*ogc* containing pSCrhaB2 empty vector alone (**Figure 1C, Supplementary Table 6** at [https://figshare.com/s/da1cee5ddc955ef29afe]). Notably, we observed that the introduction of p*ogc* did not impact glycosylation levels within *B. cenocepacia* WT regardless of induction state (**Figure 1C**). While glycosylation was observed at comparable levels within strain/plasmid combinations containing endogenous or plasmid complemented *ogc,* the proteomic analysis demonstrated OgcX and OgcA were below the limit of detection in the absence of rhamnose induction (**Figure 1D, Supplementary table 7** at [https://figshare.com/s/da1cee5ddc955ef29afe]). With the identification that p*ogc* restored glycosylation, we then sought to remove *ogcX* and *ogcA* within p*ogc* to assess the impact on viability with *ogcI* / *ogcB* removed as additional controls (**Figure 1E**). To assess the impact of *ogc* deletions on viability, we introduced plasmids into *B. cenocepacia* WT and Δ*ogc* by conjugation assessing the recovery of viable colonies. Conjugation efficiency was not impacted by the removal of *ogcA, B, I* or *X* within *B. cenocepacia* WT with comparable cfu/mL observed; however, within Δ*ogc* conjugations of p*ogc*Δ*ogcX* and p*ogc*Δ*ogcA* demonstrated dramatic reductions in recoverable cfu/mL (**Figure 1F**). These observations support that the loss of either *ogcX* and *ogcA* within p*ogc* impacts viability in the absence of chromosomally encoded *ogcX* and *ogcA*.

Deleterious effects due to the loss of *ogcX* or *ogcA* are dependent on glycosylation initiation

The absence of effects on viability in response to the loss of the *ogc* [46,62] , yet the requirement of *ogcA* / *ogcX* alone supports that if *O*-linked glycan biosynthesis is allowed to proceed, it is deleterious after the addition of the second GalNAc, mediated by the OgcB [46]. If true, we reasoned that controlling the initiation of glycosylation via placing OgcI under inducible

control should render Δ*ogcA and* Δ*ogcX* viable. To assess this, we removed *ogcI* and chromosomally re-introduced *ogcI* under rhamnose-inducible control within a miniTn7 integrative system (**Figure 2A, Supplementary Figure 1A and 1B**), generating Δ*ogcI* Tn7-*ogcI.* Proteomic and glycoproteomic analysis confirmed the inducible control of *ogcI* as well as the appearance of glycosylation upon the addition of rhamnose in this background (**Supplementary Figure 2B and 2C**). Following verification of Δ*ogcI* Tn7-*ogcI,* we generated viable mutations in *ogcX and ogcA* (Δ*ogcI*Δ*ogcX* Tn7-*ogcI* and Δ*ogcI*Δ*ogcA* Tn7-*ogcI*) as well as *ogcB and ogcAB (*Δ*ogcI*Δ*ogcB* Tn7-*ogcI* and Δ*ogcI*Δ*ogcAB* Tn7-*ogcI*, **Supplementary Figure 3**). Consistent with the requirement of glycosylation initiation to drive deleterious effects, spot plate assays in the presence of rhamnose revealed reduced growth within Δ*ogcI*Δ*ogcA* Tn7-*ogcI* and Δ*ogcI*Δ*ogcX* Tn7-*ogcI* yet did not impact Δ*ogcI*Δ*ogcAB* Tn7-ogcI*,* Δ*ogcI*Δ*ogcB* Tn7-ogcI or Δ*ogcI* Tn7-*ogcI* growth (**Figure 2B**). Quantification of colony size within strains lacking *ogcX* or *ogcA* revealed a reduction in size to 10% of Δ*ogcI* Tn7-*ogcI*, Δ*ogcI*Δ*ogcB* Tn7-*ogcI* and Δ*ogcI*Δ*ogcAB* Tn7-*ogcI* strains in response to induction (**Figure 2C**). Consistent with these results, plate-based growth assays also revealed marked delays in the growth kinetics of strains lacking *ogcX* or *ogcA* upon induction compared to Δ*ogcI* Tn7-*ogcI* (**Supplementary Figure 4**). Importantly, across strains, quantification of glycosylation using glycoproteomics supports that while rhamnose induction led to the restoration of glycosylation within Δ*ogcI* Tn7-*ogcI,* no glycosylation was observable within strains lacking *ogcA, B, X or AB* upon rhamnose induction (**Figure 2D, Supplementary Table 8** at [https://figshare.com/s/da1cee5ddc955ef29afe]).

To confirm the loss of *ogcA* and *ogcX* are the drivers of the deleterious effects upon glycosylation initiation we assessed complementation to restore protein glycosylation and viability. OgcA complementation was undertaken using the rhamnose inducible vector pScrhaB2 generating two plasmids denoted as pSCrhaB2-*ogcA*-Met1 (p*ogcA*$_{Met1}$) and pSCrhaB2-*ogcA*-Met2 (p*ogcA*$_{Met2}$) corresponding to variants differing in the two potential start codons of *ogcA* (**Supplementary Figure 5A**). Spot assays revealed the introduction of either p*ogcA*$_{Met1}$ or p*ogcA*$_{Met2}$ into Δ*ogcI*Δ*ogcA* Tn7-*ogcI* restored viability and colony size compared to a pSCrhaB2 empty vector control (**Figure 3A, Supplementary Figure 5B**). Proteomics and glycoproteomic analysis further confirmed both the induction of OgcA and restoration of glycosylation to comparable levels to Δ*ogcI* Tn7-*ogcI* from Δ*ogcI*Δ*ogcA* Tn7-*ogcI*

containing p*ogcA*$_{Met1}$ or p*ogcA*$_{Met2}$ in a rhamnose dependent manner with neither OgcA nor glycosylation detected within Δ*ogcI*Δ*ogcA* Tn7-*ogcI* strain containing pSCrhaB2 (**Figure 3B-C, Supplementary Table 9 and 10** at [https://figshare.com/s/da1cee5ddc955ef29afe]). Critically, proteomic and glycoproteomic analysis of Δ*ogcI*Δ*ogcA* Tn7-*ogcI* containing pSCrhaB2 under rhamnose induction was unable to be assessed due to loss of viability. To complement *ogcX,* we generated a modified pMLBAD vector [69] that placed *ogcX* expression under cumate induction. The resulting pCumate-*ogcX-his* (p*ogcX*) and the control vector (pCumate-sfGFP, p*sfGFP*) were introduced into Δ*ogcI* Tn7-*ogcI* as well as Δ*ogcI*Δ*ogcX* Tn7-*ogcI* and viability assessed using spot assays with rhamnose / cumate induction. Akin to *ogcA* complementation, the introduction of p*ogcX* into Δ*ogcI*Δ*ogcX* Tn7-*ogcI*, followed by rhamnose induction of OgcI, restored viability and colony size observed compared to p*sfGFP* (**Figure 3D**). Notably, the presence of p*ogcX* regardless of induction was sufficient to relieve the deleterious effects from the initiation of glycosylation (**Supplementary Figure 5C**). Glycoproteomics confirmed the restoration of glycosylation of Δ*ogcI*Δ*ogcX* Tn7-*ogcI* containing p*ogcX* in a rhamnose-dependent manner and the absence of glycosylation within Δ*ogcI*Δ*ogcX* Tn7-*ogcI* containing p*sfGFP* (**Figure 3E, Supplementary Table 11** at [https://figshare.com/s/da1cee5ddc955ef29afe]). As observed within *ogcA* complementation, proteomic/glycoproteomic analysis of Δ*ogcI*Δ*ogcX* Tn7-*ogcI* containing p*sfGFP* under rhamnose induction was unable to be assessed due to loss of viability (**Figure 3E/F**). Additionally, proteomic analysis confirms OgcX induction from p*ogcX* revealed a low-level of OgcX production even in the absence of cumate induction (**Figure 3F, Supplementary Table 12** at [https://figshare.com/s/da1cee5ddc955ef29afe]), confirming that pSCrhaB2 has a low level of gene leakage. Combined, these complementation assays support that the loss of *ogcA* and *ogcX* are the drivers of the deleterious effects on the viability of *B. cenocepacia* upon glycosylation initiation.

Proteomic analysis reveals loss of *ogcX* or *ogcA* drives alterations within the membrane proteome

Our initial proteomic characterisations (**Figure 1D, 3A, 3F**) revealed variability in tracking proteins of the OGC; thus, to improve the depth and reproducibility of protein quantification of these proteins, we turned to the use of Data-Independent Acquisition (DIA) based

proteomics [100,101]. To understand the proteomic changes uniquely driven by loss of *ogcX* and *ogcA* we compared the proteome of four strains Δ*ogcI* Tn7-*ogcI,* Δ*ogcI*Δ*ogcA* Tn7-*ogcI,* Δ*ogcI*Δ*ogcB* Tn7-*ogcI and* Δ*ogcI*Δ*ogcX* Tn7-*ogcI* under both rhamnose induced and non-induced conditions. Using DIA proteomic analysis, all five proteins of the OGC were observed allowing the confirmation of the expected loss of OGC proteins (**Supplementary Figure 6, Supplementary Table 13** at [https://figshare.com/s/da1cee5ddc955ef29afe]). Across strains, a total of 3748 proteins were identified, with ~90% identified with >2 unique peptides in each biological replicate (**Supplementary Figure 7A**). Principal component analysis revealed distinct clustering for each biological group, with the Δ*ogcI*Δ*ogcA* Tn7-*ogcI* and Δ*ogcI*Δ*ogcX* Tn7-*ogcI* strains separating along PC1 upon induction supporting the loss of these genes leading to similar overall proteomic effects when glycosylation is initiated (**Figure 4A**). Examination of the protein alterations between non-induced and induced conditions revealed that induction resulted in significant changes (defined as >2-fold difference and -log10(p-value) > 2) within strains lacking *ogcX* and *ogcA* while relatively few alterations were observed within Δ*ogcI*Δ*ogcB* Tn7-*ogcI* and Δ*ogcI* Tn7-*ogcI* (**Figure 4B**). Across the alterations observed in Δ*ogcI*Δ*ogcX* Tn7-*ogcI* and Δ*ogcI*Δ*ogcA* Tn7-*ogcI*, 722 proteins were differentially impacted in both, with Δ*ogcI*Δ*ogcX* Tn7-*ogcI* exhibiting the highest number of overall protein alterations (**Figure 4C**). Notably, the protein alterations within impacted proteins within Δ*ogcI*Δ*ogcX* Tn7-*ogcI* and Δ*ogcI*Δ*ogcA* Tn7-*ogcI* were highly similar, demonstrating significant co-enrichment (Fisher exact test Benjamini-Hochberg corrected *p*-value = $8.20*10^{-204}$, **Supplementary Figure 7B and Supplementary Table 14** at [https://figshare.com/s/da1cee5ddc955ef29afe]). To assess the overall patterns within the observed protein alterations, Gene Ontology (GO) enrichment was undertaken on the proteome alterations observed within Δ*ogcI*Δ*ogcX* Tn7-*ogcI,* revealing an over-representation of membrane-associated protein classes (**Figure 4D, Supplementary Table 14** at [https://figshare.com/s/da1cee5ddc955ef29afe]). Combined DIA proteomic analysis supports that the disruption of *ogcX* and *ogcA* leads to similar and widespread proteomic alterations characterised by dramatic changes in the membrane proteome when glycosylation is initiated.

Loss of *ogcA* and *ogcX* impacts membrane integrity and permeability within *B. cenocepacia*

Given the dramatic proteomic alterations in response to the loss of *ogcX* and *ogcA* with induction of glycosylation, we hypothesised that these changes could drive alterations in membrane integrity akin to changes noted within other Wzx-dependent glycan pathways [4,6,7,33,102]. Thus, to assess membrane integrity, we assayed the impact of membrane (0.01% SDS) and osmotic (2% NaCl) stresses on glycosylation inducible strains. Within *ogcX* and *ogcA* deletion strains, spot plate assays revealed increased sensitivity to 0.01% SDS upon glycosylation initiation compared to the absence of initiation yet minimal effect on strains lacking *ogcB* or *ogcAB* (**Figure 5A**). In contrast, all strains were adversely impacted by osmotic stress (2% NaCl) in the absence of induction, yet only *ogcX* and *ogcA* deletion strains failed to show improved viability following glycosylation induction (**Figure 5A**). Plate-based growth assays recapitulated these observations with the deletion of *ogcX* and *ogcA,* demonstrating alterations in growth kinetics in the presence of 0.01% SDS or 2% NaCl (**Supplementary Figure 8**). These observations support the loss of membrane integrity within Δ*ogcX* and Δ*ogcA* backgrounds in response to known stressors. To directly assess membrane permeability in response to glycosylation, we undertook Hoechst 33342 and N-phenyl-1-naphthylamine (NPN) fluorescesent-based permeability assays. Utilising Hoechst 33342, a fluorescent DNA binding dye, we evaluated Hoechst 33342 uptake, revealing enhanced fluorescence within Δ*ogcX* and Δ*ogcA* backgrounds upon glycosylation initiation, yet minimal alterations in other strains (**Figure 5B**). Similarly, NPN uptake assays, which monitor dye partitioning into membranes [82], revealed increased fluorescence in Δ*ogcI*Δ*ogcX* Tn7-*ogcI* and Δ*ogcI*Δ*ogcA* Tn7-*ogcI* strains under induced conditions, supporting increased membrane permeability (**Figure 5C**). Critically, the assessment of strain viability supports these alterations are due to changes in membrane integrity and not lysis, with cells used for analysis containing comparable viable bacterial numbers (**Supplementary Figure 9**). Combined, these findings support that the loss of *ogcX* and *ogcA* compromises the *B. cenocepacia* envelope, leading to sensitisation to stressors and membrane permeability.

Loss of *ogcA* and *ogcX* enhances sensitivity of *B. cenocepacia* to antimicrobials

The observations that the loss of *ogcX* and *ogcA* leads to widespread impacts on the *B. cenocepacia* membrane highlight the potential for these effects to be exploited to potentiate antimicrobial agents. In line with this, recent transposon studies have suggested

that mutations within the *ogc* alter susceptibility to β-lactam antibiotics; however, validation of these effects using CRISPRi resulted in only modest recapitulation of sensitization [60]. Given that our prior experiments (**Figure 3A and D**) indicate enhanced sensitivity of *ogcX* and *ogcA* strains to trimethoprim, we assessed the impact of antimicrobial agents including trimethoprim, tetracycline, ceftazidime, chlorhexidine and rifampicin on glycosylation inducible strains. Utilising broth dilution assays, changes in antimicrobial sensitivity were observed in strains lacking *ogcX* and *ogcA* upon induction yet were modest in magnitude corresponding to a 1- to 2-fold decrease in the minimal inhibitory concentrations (MIC) of trimethoprim and ceftazidime (**Supplementary Figure 10 and Supplementary Table 5**). To improve the detection of alterations in antimicrobial sensitivity, we assessed the impact of antimicrobial agents at or below the broth dilution-defined MICs using spot assays. Utilising this approach, no effect on growth was observed with chlorhexidine, yet upon induction, strains lacking *ogcX* and *ogcA* were observed to show enhanced sensitivity to tetracycline, rifampicin, trimethoprim and ceftazidime compared to Δ*ogcI*Δ*ogcB* Tn7-*ogcI* and Δ*ogcI* Tn7-*ogcI* (**Figure 6**). Interestingly, for both trimethoprim and ceftazidime, all strains showed reduced growth without induction, yet the growth of Δ*ogcI*Δ*ogcB* Tn7-*ogcI* and Δ*ogcI* Tn7-*ogcI* was improved upon induction (**Figure 6**). Combined, these findings support the loss of *OGC* genes appears to sensitise *B. cenocepacia* to several antimicrobial agents with these impacts most pronounced for strains lacking *ogcX* or *ogcA* upon initiation of glycosylation.

Modulation of Und-P/Und-PP precursor levels and early *ogc* biosynthesis steps impacts the viability of *B. cenocepacia*

As the deletion of *ogcA* and *ogcX* leads to deleterious effects upon glycosylation initiation, we questioned if Und-P/Und-PP sequestration may be responsible for driving these effects, as noted within other Und-P/Und-PP-dependent glycan pathways [6,7]. We reasoned that modulating Und-P precursor levels as well as Und-PP-bound intermediates, especially during early steps in *O*-linked glycan biosynthesis, may alter viability within *B. cenocepacia.* To probe this, we overexpressed undecaprenyl pyrophosphate synthase (UppS), the *de novo* synthase responsible for generating UndP, which has been previously shown to relieve UndP sequestration (**Figure 7A**) [7,103]. Utilising cumate-inducible vectors containing the two putative annotated UppS enzymes of *B. cenocepacia* K56-2*,* BCAL2087 and BCAM2067 creating the

vectors pBCAL2087 and pBCAM2067 respectively, we assessed the impact of UppS overexpression in the absence of *ogcA* and *ogcX* with glycosylation initiation. Within strains lacking *ogcA* and *ogcX*, the induction of pBCAL2087 partially alleviated reductions observed within Δ*ogcA* and Δ*ogcX* backgrounds, while pBCAM2067 only restored viability within Δ*ogcI*Δ*ogcA* Tn7-*ogcI* (**Figure 7B**). Despite the observed reduced colony sizes noted within pBCAL2087, quantification revealed comparable levels of colonies observed within strains upon induction with both cumate and rhamnose compared to non-induced conditions (**Figure 7C**). To probe if alterations in Und-PP-bound intermediates may modulate viability, we overexpressed components of the *ogc* within the parental *B. cenocepacia* K56-2 background. Introduction of rhamnose inducible vectors containing *ogcI* (p*ogcI*), *ogcB* (p*ogcB*), *ogcA* (p$ogcA_{Met1}$) as well as an inducible vector containing both *ogcA* and *ogcB* (p$ogcAB_{Met1}$) revealed induction of p*ogcI* and p*ogcB* resulted in reduced viability, while the overexpression of *ogcA*(p*ogcA*),*ogcAB* (p*ogcAB*), and the complete *ogc* (p*ogc*) showed no impact on viability (**Figure 7D-E**). Critically, complementation of *B. cenocepacia* Δ*ogcAB,* Δ*ogcB* and Δ*ogcI* with p$ogcAB_{Met1}$, p*ogcB* and p*ogcI* induced with 0.05% rhamnose restored glycosylation, confirming the functionality of these constructs (**Supplementary Figure 11 to 13 and Supplementary Table 15 to 20** at [https://figshare.com/s/da1cee5ddc955ef29afe]). These observations support that the overexpression of early steps in *O*-linked glycan biosynthesis, OgcI and OgcB, appear to impact viability, yet these effects can be alleviated in the case of *ogcB* by co-expression of *ogcA*. Combined, these observations support alterations in both Und-P/Und-PP levels, as well as early steps in *O*-linked glycan biosynthesis, modulate *ogc*-associated viability, supporting Und-P/Und-PP sequestration as the likely cause of deleterious effects from the loss of *ogcA* and *ogcX*.

Discussion:

Burkholderia O-linked glycosylation, mediated by the *OGC* and *pglL* [46,58], are highly conserved at a pathway and glycan composition levels [44-46]. While previous work demonstrated the requirement of the *OGC* for the generation of the trisaccharide used for glycosylation [46], a deeper understanding of how glycan fidelity is controlled, as well as the impact of *ogcA* and *ogcX* on *B. cenocepacia* has not been assessed. In line with the growing recognition of the impact of Und-P/ Und-PP sequestration by dead-end intermediates of O-antigens [6,11], capsule [34] and the ECA [7,10] glycans, we demostrate that blocking *OGC* also appears to lead to sequestration of the Und-P/ Und-PP pool. Critically, this work highlights that in line with previous studies on Wzx-dependent glycan pathways [3,4,10,27], the *B. cenocepacia O*-linked glycosylation pathway appears highly selective for its complete cognate glycan. This observation sheds light on the near-exclusive presence of the observed Hex–HexNAc–HexNAc structure decorating glycoproteins within all *Burkholderia* glycoproteomic studies to date [45,46,58,87,104,105] and suggests glycan selectivity is of functional importance.

The conservation of the *Burkholderia O*-linked glycan makes this glycosylation system unique among characterised bacterial protein glycosylation systems to date, including the *O*-linked glycosylation systems of *Acinetobacter* [106-108] and *Neisseria* [39,57,109], as well as the *N*-linked glycosylation systems of *Campylobacter* [37,38] where extensive glycan diversity has been reported. While the conservation of glycans in the context of protein glycosylation systems appears atypical, the conservation of glycan biosynthesis across species, or even genera, has previously been noted, as in the case of the ECA [110,111]. For the ECA, it has been suggested that the invariance of this oligosaccharide underpins its importance to *Enterobacterale* physiology [111]. While the function of *Burkholderia O*-linked glycosylation is still unknown, this work raises a critical question on the importance of the cognate glycan in glycosylation. Despite the identification of *B. cenocepacia* glycosylation over a decade ago, we have yet to identify a specific function for glycosylation, nor have individual glycosylation events been identified that require glycosylation for functionality [58,62,105]. As it has been demonstrated that Wzx flippases can be altered to allow translocation of non-native substrates [14-16] this suggests that modification of OgcX may allow the uncoupling of glycosylation from the impacts mediated by modification with non-cognate structures. Thus, the generation of the tools and

strains in this study provides an important starting point for exploring OgcX specificity, as well as understanding how the loss of glycan fidelity may impact *Burkholderia* physiology.

Our observations of deleterious effects in response to the loss of *ogcX* (**Figure 1, 2 & 3**) suggest the previously reported Δ*ogcX* isolate within *B. cenocepacia* [46] likely possessed an uncharacterised suppressor mutation. As noted previously, suppressor mutations can rapidly emerge upon Und-P/Und-PP sequestration [9,32,33] with the emergence of a potential suppressor mutation highlighted as the potential source of confounding results associated with defining the function of the WzxE flippase within *E. coli* K-12 [10]. While we were unable to obtain the previously reported Δ*ogcX* isolate the observation that low-level glycosylation of a truncated glycan of a single HexNAc residue within this strain [46], suggests a potential disruption within the *O*-linked glycosylation system of this isolate. In contrast to previous results, our observation of the requirement of OgcX for *O*-glycosylation supports that this flippase is indispensable within *B. cenocepacia* for translocation of the *O*-linked glycan into the periplasmic space. Interestingly, not all flippases are indispensable as has been noted within *E. coli* K-12, where some redundancy exists in the ability of ECA to be mobilised to the periplasm by the O-antigen (Wzx_{O16}) or colanic acid (WzxC) flippases [112]. Our analysis of glycosylation in the absence of *ogcX* (**Figure 2D**) is consistent with a lack of functional redundancy for the cognate *O*-linked glycan by the remaining Wzx flippases of *B. cenocepacia.* Within *B. cenocepacia* K56-2, previous analysis has highlighted the presence of at least five putative Wzx flippases with similar functional indispensability observed for the peptidoglycan flippase $murJ_{Bc}$ (BCAL2764) [113]. Thus, these findings support that OgcX is the sole flippase required for translocation of the *O*-linked glycan, and alternative flippases are not functionally redundant for this glycan in *B. cenocepacia.*

We have previously reported the inability to generate Δ*ogcA* within *B. cenocepacia* [46], yet disruptions of *ogcA* were recently suggested to be tolerated [60]. Our data assessing the loss of *ogcA* using plasmid-based complementation (**Figure 1**) as well as strains with inducible control of glycosylation (**Figure 2-3**) supports that, akin to *ogcX*, the loss of *ogcA* is deleterious within *B. cenocepacia*. Previously, putative Δ*ogcA* candidates were observed within high-density transposon libraries yet *ogcA* CRISPRi silencing failed to recapitulate the resulting phenotypes associated with Δ*ogcA* [60]. As such, we suggest that the Δ*ogcA* reported within

prior work may contain unexpected secondary mutations or that the presence of transposons within *ogcA* may have adversely affected the expression of neighbouring genes of the *ogc*. While transposon libraries coupled with sequencing provide a robust means to assess gene function at a genomic scale [114], it is recognised that this approach can lead to inactivation or polar effects in neighbouring genes [115,116]. Furthermore, the enrichment of transposon junctions prior to sequencing [114] does not allow the assessment of unlinked potential suppressor or inactivation events, which may restore variability even in the presence of insertions into conditionally essential genes. Of note within our work, the utilisation of proteomics allowed the assessment of *ogcA*, ogc*X,* and ogc*B* mutagenesis, revealing neighbouring *ogc* proteins are unaffected by the removal of these genes (**Supplementary Figure 6**). Considering our findings, in addition to prior transposons studies of *B. cenocepacia* and *Burkholderia pseudomallei* that assign *ogcA* as essential [59,61], this supports the assignment of *ogcA* as conditionally essential.

The observation that both *ogcA* and *ogcX* appear conditionally deleterious/essential is consistent with a growing body of work highlighting the detrimental impacts of blocking Und-P/PP biosynthetic pathways [6,7,11]. As within previous studies on the deleterious impacts of Und-P/PP sequestration, the use of inducible systems [10,11,14] provided a tractable way to explore the roles of *ogcA*/*ogcX* while limiting potential confounding effects from the emergence of suppressors. The inducible deleterious effects from the loss of *ogcA* and *ogcX* (**Figure 2**) support fouling of the Und-P/PP pool with complementation confirming the restoration of glycosylation as well as suppression of growth defects by the re-introduction of *ogcX* / *ogcA* (**Figure 3**). Interestingly, within this work, we noted that while introduction of plasmid variants lacking *ogcA/X* were unable to be recovered from *B. cenocepacia,* Δ*ogc* rhamnose inducible strains lacking *ogcA/X* were viable although exhibited reduced growth rates (**Figure 2, Supplementary Figure 4**). While the viability of inducible Δ*ogcA and* Δ*ogcX* strains was essential for allowing proteomic (**Figure 4**) and phenotypic assessments (**Figure 5, 6 and 7**), this does suggest the overall restoration of glycosylation mediated by Tn7-rha-*ogcI* may be reduced compared to wild type *B. cenocepacia,* reducing the magnitude of the effect of sequestration on the Und-P/PP pool. In line with this, we noted higher overall glycosylation levels, as determined by identified glycopeptides, within wildtype *B. cenocepacia* (**Figure 1C**) compared to the observed levels within glycosylation inducible strains (**Figure 2D, 3C and 3F**)

consistent with an overall reduced glycosylation capacity. Regardless, the ability to demonstrate changes in membrane permeability and stress sensitivity (**Figures 5 and 6**) highlights the importance of *O*-linked glycan completion for *B. cenocepacia* physiology. Importantly, this also allowed the assessment of antibiotic sensitisation previously suggested for Δ*ogcA* [60], expanding on this observation and highlighting that both Δ*ogcA and* Δ*ogcX,* upon initiation of glycosylation, sensitise *B. cenocepacia* to clinically important antibiotics including tetracycline, rifampicin, trimethoprim as well as ceftazidime (**Figure 6**). This finding supports that fouling of the Und-P/PP pool through the inhibition of *ogcA* or *ogcX* may be a potent way to sensitise *Burkholderia* to antibiotics. The concept of modulating the Und-P/PP pool to sensitise *B. cenocepacia* has been previously explored by the depletion of *dxr* (BCAL2085) [117], which directly contributes to the precursors required for UppS-mediated *de novo* synthesis of Und-P [1,118]. Thus, fouling of the Und-P/PP pool through inhibition of OgcX or OgcA may be an attractive approach for drug re-sensitisation.

Our work provides multiple lines of evidence (**Figure 1-5**) supporting Und-P/PP fouling as the driver of the defects observed within Δ*ogcA* and Δ*ogcX* yet it should be noted that despite multiple attempts, the direct tracking of the Und-P/PP pools within *B. cenocepacia* has been unsuccessful within our hands. While recent progress has been made in the direct analysis of Und-P sequestration products [119] to further support the involvement of Und-P we turned to the overexpression of UppS, which has been demonstrated to reverse the phenotypic defects caused by the generation of dead-end intermediates [7]. Our analysis supports the overexpression of BCAL2087 partially restores growth in both Δ*ogcA* and Δ*ogcX* backgrounds, making this the likely primary UppS of *B. cenocepacia* (**Figure 7**). Consistent with the assignment of BCAL2087 as UppS within *B. cenocepacia,* BCAL2087 is assigned as essential within transposon library studies [59,60], and CRISPRi silencing of this gene is associated with growth inhibition [60]. While overexpression of UppS relieved growth inhibition, our analysis of individual *ogc* components revealed OgcI and OgcB also inhibited growth when overexpressed within *B. cenocepacia,* yet these proteins do not themselves impact growth within *E. coli* (**Supplementary Figure 14**). The ability of induction of *ogcB* and *ogcI* with 0.05% rhamnose to restore glycosylation within *B. cenocepacia* Δ*ogcB* and Δ*ogcI* strains (**Supplementary Figure 12 and 13**) yet to lead to toxicity at higher levels of induction (1% rhamnose) supports that OgcI and OgcB themselves are not toxic but likely increase the

proportion of early-stage intermediates in *OGC* biosynthesis driving the sequestration of the Und-PP/P pool. Consistent with this model, the overexpression of OgcA and OgcB was found to relieve toxicity (**Figure 7**), supporting the sensitivity of the *B. cenocepacia* Und-P/PP pool to changes in *ogc* intermediate levels. It should be noted a caveat of our model is the assumption that the products of the *ogc* solely supply glycan units used for protein glycosylation, yet whether this is the case is unknown. As noted within other glycan biosynthesis pathways both glycan intermediates as well as complete glycan units may be incorporated into different glycoconjugates [110,111]. Previous studies of *O*-linked glycosylation systems have demonstrated that glycans used for glycosylation may be derived from several Und-P-dependent biosynthesis pathways, such as the O-antigen in *Pseudomonas aeruginosa* [120,121] and capsule pathways in family of the *Moraxellaceae* [122,123]. In light of this, while the OGC is sufficient and required for protein glycosylation [46] and we show the modulation of *OGC* intermediates impact viability, it is currently unclear if this pathway contributes solely to protein glycosylation, which impacts the interpretation of these findings.

In conclusion, this work demonstrates that the loss of *ogcA*/*X* within *B. cenocepacia* results in detrimental impacts on viability, membrane permeability and the proteome, which appears to sensitise strains to membrane stresses as well as clinically useful antibiotics. These findings not only advance our understanding of *Burkholderia O*-linked protein glycan biosynthesis but also highlight the therapeutic potential of targeting the *O*-linked glycan biosynthesis pathway. Finally, this work highlights that akin to the impacts of glycan biosynthesis blockages observed in O-antigens [6,9] and the ECA [7,10], modulating or blocking the generation of OGC intermediates appears to lead to sequestration of the Und-P/PP pool within *B. cenocepacia.*

Acknowledgements:

N.E.S is supported by an Australian Research Council (ARC) Future Fellowship (FT200100270), an ARC Discovery Project Grant (DP210100362) and a National Health and Medical Research Council Ideas grant (2018980). We thank the Melbourne Mass Spectrometry and Proteomics Facility of The Bio21 Molecular Science and Biotechnology Institute for access to MS instrumentation. We thank Nicholas Coleman for sharing the plasmid pUS250-sfGFP and Erin Garcia for sharing the plasmid pFlptet.

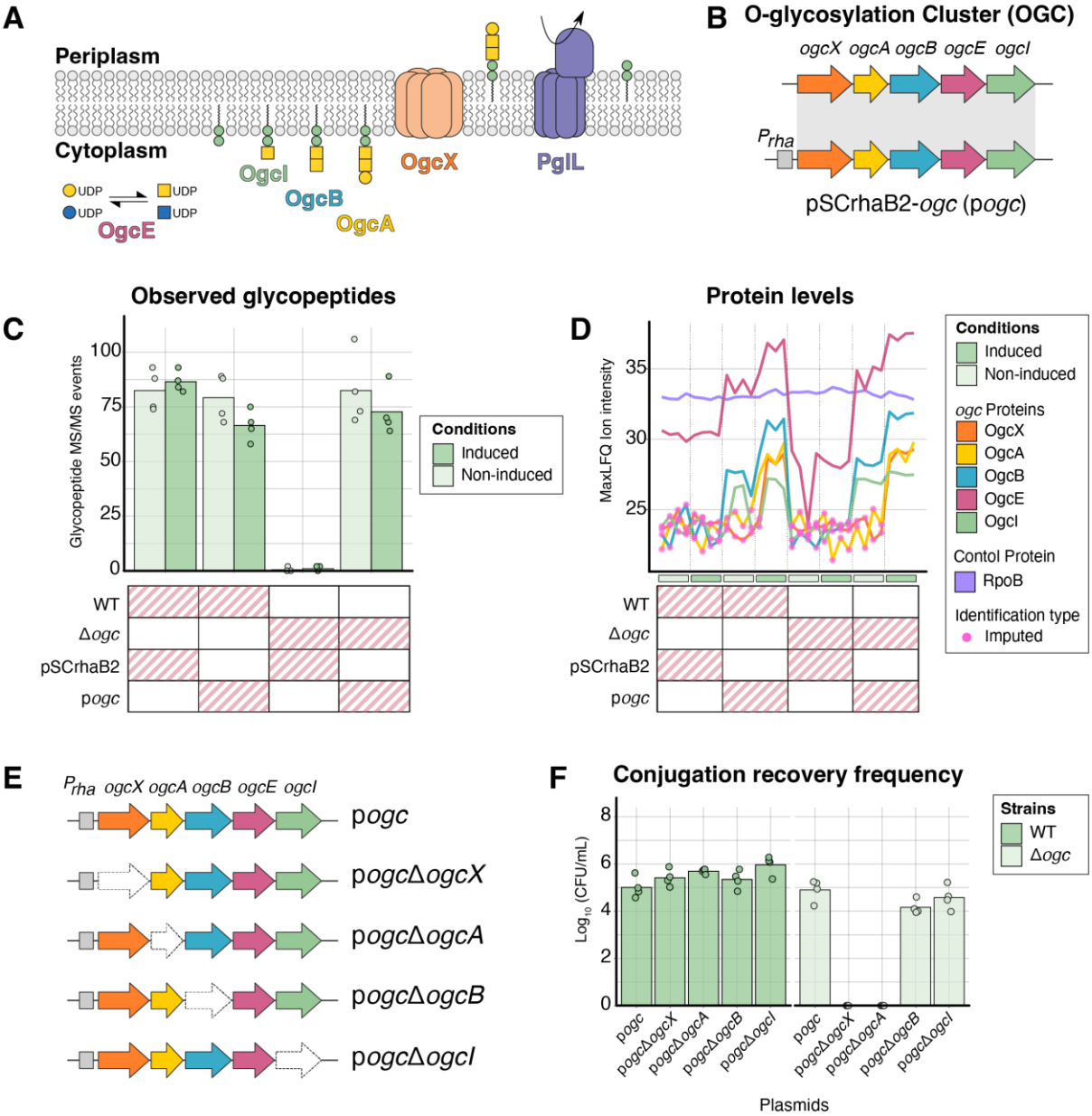

Figure 1. Loss of *ogc*X and *ogc*A impacts viability of *B. cenocepacia* Δ*ogc*. A) diagram of the *O*-glycosylation biosynthesis pathway in *Burkholderia* species [46]. *O*-glycosylation biosynthesis involves the stepwise construction of a conserved trisaccharide by the glycosyltransferases, OgcI, OgcB and OgcA, with the nucleotide-sugar donors UDP-GalNAc and UDP-Gal generated by the epimerase OgcE. The resulting trisaccharide is then thought to be translocated across the inner membrane by the putative flippase, OgcX. Once in the periplasm, the glycans can be transferred to proteins by the oligosaccharyltransferase, PglL. **B)** Graphic representation of the genetic organization of the *ogc* cluster (*ogc*X, A, B, E and I assigned as BCAL3114–BCAL3118 within *B. cenocepacia* J2315) and its integration into the rhamnose-inducible vector pSCrhaB2, resulting in the generation of the pSCrhaB2-*ogc* (p*ogc*). **C-D)** Quantification

of glycopeptides and proteins encoded by the *ogc* cluster identified from whole cell proteomic analysis of *B. cenocepacia* WT and Δ*ogc* containing either pSCrhaB2 or p*ogc* with and without induction with 1% rhamnose (n=4). **E)** Graphic representation of p*ogc* mutagenesis removing *ogc*X, *ogc*A, *ogc*B and *ogc*I. **F)** Conjugation of p*ogc* derivatives into *B. cenocepacia* K56-2 WT and Δ*ogc* reveals differences in recovery rates of p*ogc*Δ*ogc*X and p*ogc*Δ*ogc*A within *B. cenocepacia* Δ*ogc* (n=4).

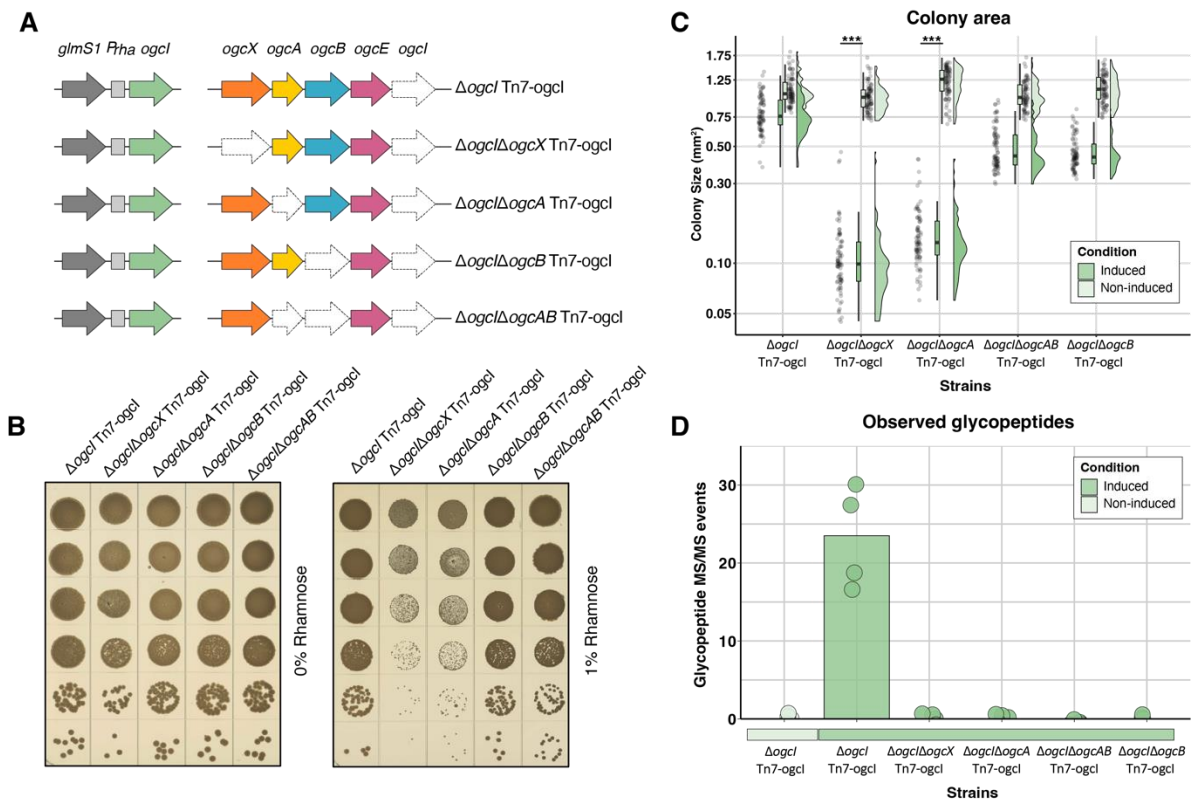

Figure 2. Loss of *ogcX* or *ogcA* leads to reduced growth when glycosylation is initiated. A) Graphic representation of strains Δ*ogcX, ΔogcA, ΔogcB and ΔogcAB* generated within the chromosomal inducible background *B. cenocepacia* Δ*ogcI* Tn7-*ogcI*. **B-C)** Spot plate assays and half-violin box plots assessing growth of strains with and without 1% rhamnose induction. Induction results in reduced colony size of Δ*ogcX* and Δ*ogcA* strains to 10% of the size observed in *B. cenocepacia* Δ*ogcI* Tn7-*ogcI* and strains without induction (n=4). **D)** Quantification of glycopeptides identified from whole-cell proteomic analysis of strains. Glycopeptides were assessed in the absence (light green) or presence (dark green) of rhamnose induction (n=4). Induction of *ogcI* expression by 1% rhamnose led to the restoration of glycosylation only in *B. cenocepacia* Δ*ogcI* Tn7-*ogcI* in contrast, no glycosylation was observed in the Δ*ogcX*, Δ*ogcB*, and Δ*ogcAB* strains.

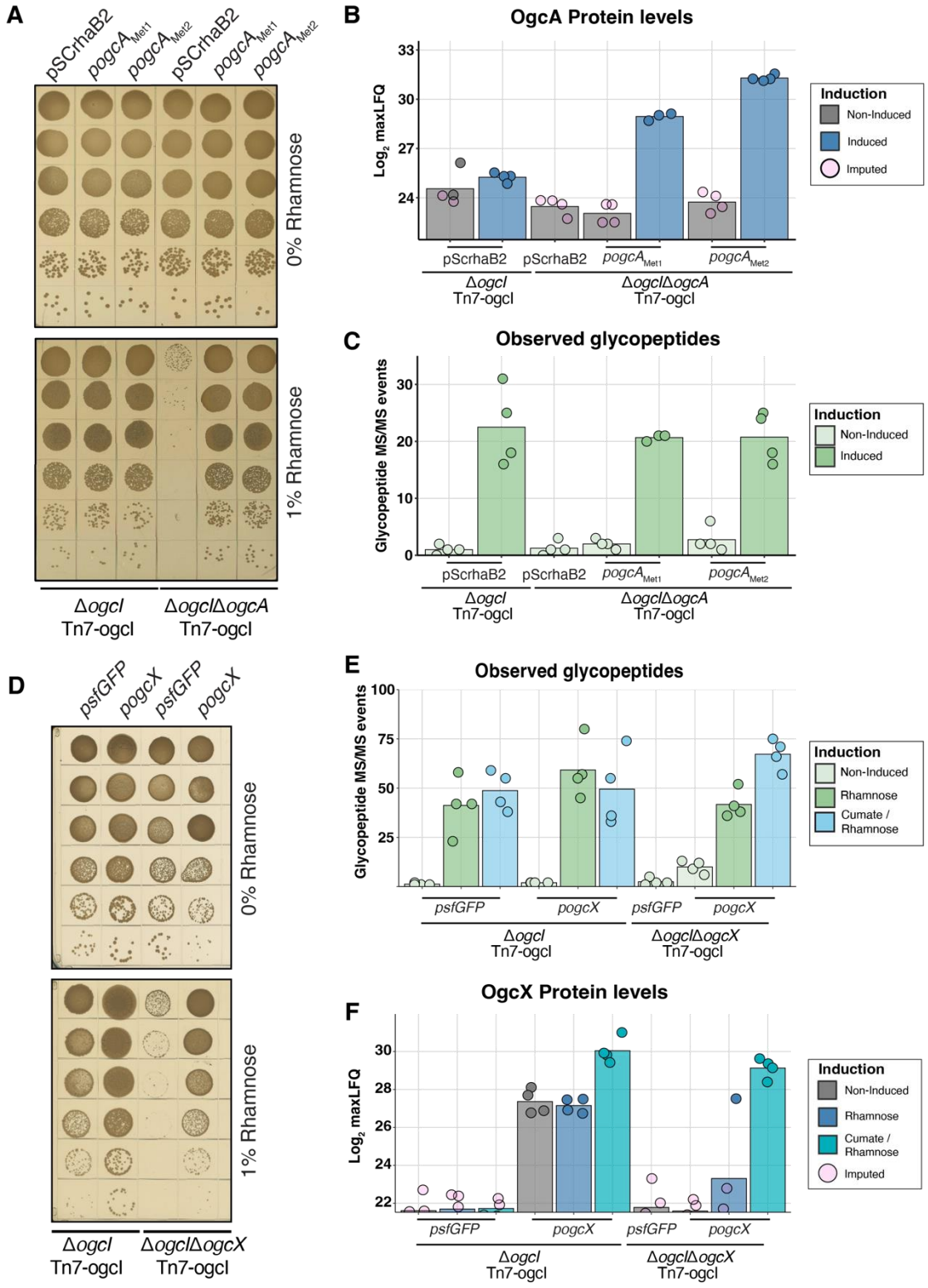

Figure 3. Complementation of Δ*ogcA* and Δ*ogcX* restores growth and glycosylation. A) Spot plate assays of *B. cenocepacia* Δ*ogcI* Tn7-*ogcI* and *B. cenocepacia* Δ*ogcI*Δ*ogcA* Tn7-*ogcI* containing pSCrhaB2 (EV), pSCrhaB2-*ogcA*-Met1 (*ogcA*-Met1), or pSCrhaB2-*ogcA*-Met2 (*ogcA*-Met2) with and without 1% rhamnose induction revealing complementation of Δ*ogcA* with *ogcA* variants restores viability and colony size. **B-C)** Quantification of glycopeptides and

OgcA levels from whole-cell proteomic analysis of *B. cenocepacia* Δ*ogcI* Tn7-*ogcI* and *B. cenocepacia* Δ*ogcI*Δ*ogcA* Tn7-*ogcI* strains carrying EV, $ogcA_{Met1}$, or $ogcA_{Met2}$. Induction results in the detection of OgcA within *B. cenocepacia* Δ*ogcI*Δ*ogcA* Tn7-*ogcI* and the restoration of glycosylation (n=4, Δ*ogcI* Δ*ogcA* Tn7-*ogcI ogcA*-Met1 induced group n=3). **D)** Spot plate assays of *B. cenocepacia* Δ*ogcI* Tn7-*ogcI* and *B. cenocepacia* Δ*ogcI*Δ*ogcX* Tn7-*ogcI* carrying pcumate-sfGFP (sfGFP) and pcumate-*ogcX-his* (p*ogc*X) with and without 1% rhamnose induction revealing complemented Δ*ogcX* restores viability and colony size. **E-F)** Quantification of glycopeptides and OgcX levels from whole-cell proteomic analysis of *B. cenocepacia* Δ*ogcI* Tn7-*ogcI* and *B. cenocepacia* Δ*ogcI*Δ*ogcX* Tn7-*ogcI* strains carrying sfGFP or *ogcX* plasmids. Induction results in the detection of OgcX within *B. cenocepacia* Δ*ogcI*Δ*ogcX* Tn7-*ogcI* and the restoration of glycosylation (n=4).

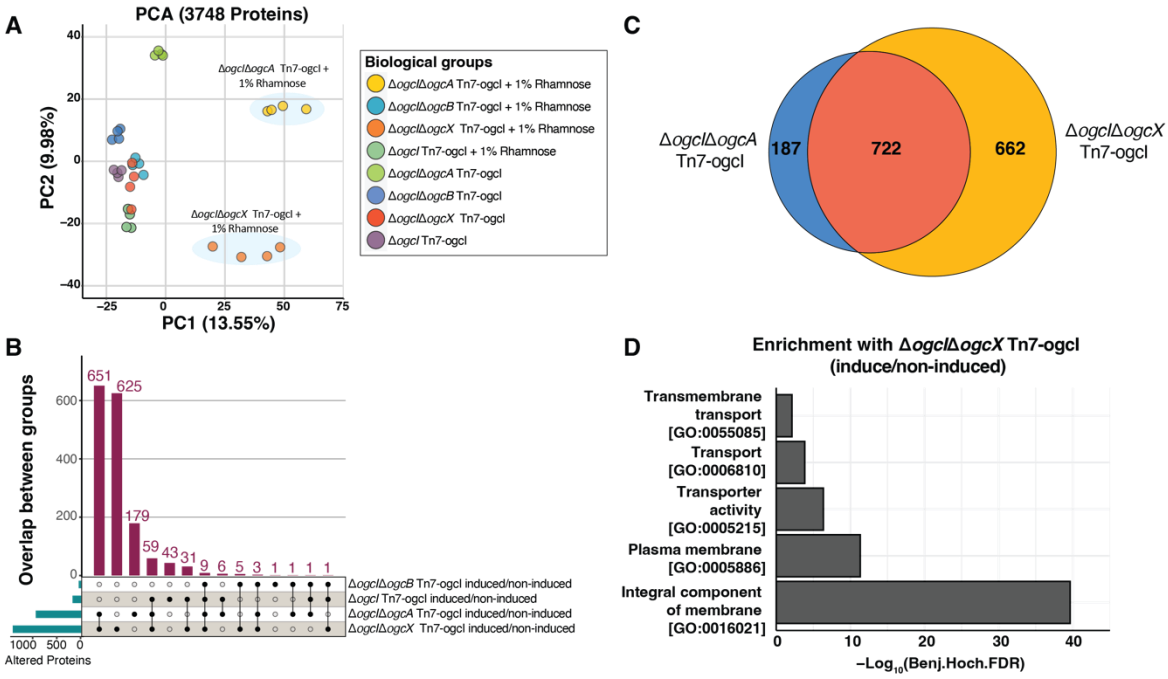

Figure 4. Proteomic analysis of strains in response to glycosylation initiation. DIA proteomic analysis of Δ*ogcI* Tn7-ogcI, Δ*ogcI*Δ*ogcA* Tn7-*ogcI*, Δ*ogcI*Δ*ogcB* Tn7-*ogcI*, and Δ*ogcI*Δ*ogcX* Tn7-*ogcI* strains with and without rhamnose induction (n=4). **A)** Principal component analysis (PCA) of Δ*ogcI* Tn7-*ogcI* strains under induced and non-induced conditions. Biological groups are observed to form distinct clusters, with Δ*ogcI*Δ*ogcA* Tn7-*ogcI* and Δ*ogcI*Δ*ogcX* Tn7-*ogcI* strains separating along PC1 upon induction. **B-C)** Upset plot and Venn diagram of proteomic alterations, defined as >2-fold-change and -$\log_{10}$(p-value) > 2 observed across strains, reveal that induction results in hundreds of protein alterations within Δ*ogcI*Δ*ogcA* Tn7-*ogcI* and Δ*ogcI*Δ*ogcX* Tn7-*ogcI* strains compared to Δ*ogcI*Δ*ogcB* Tn7-*ogcI* or Δ*ogcI* Tn7-ogcI. **D)** Enrichment analysis of GO terms associated with the altered proteins in the Δ*ogcI*Δ*ogcX* Tn7-*ogcI* strain reveals an over-representation of proteomic changes in membrane-associated protein classes.

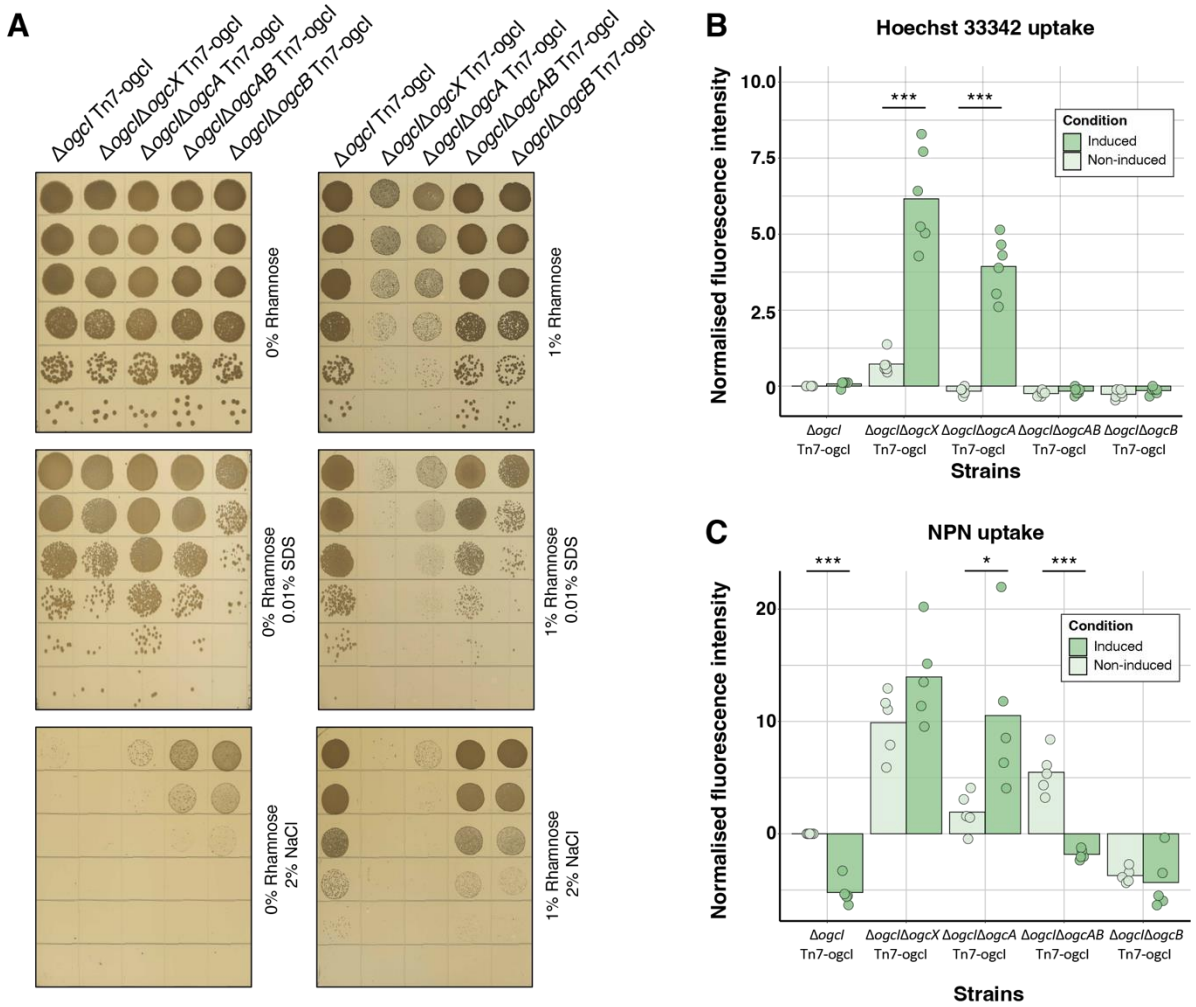

Figure 5. Loss of *ogcA* and *ogcX* impacts the membrane integrity of *B. cenocepacia*. A) Spot plate assays of strains in response to membrane (0.01% SDS) and osmotic (2% NaCl) stress with and without 1% rhamnose induction (n=4). The deletion of ogcX and *ogcA* increases sensitivity to 0.01% SDS when glycosylation is initiated, while both mutants appear sensitive to osmotic stress (2% NaCl) regardless of induction. **(B-C)** Hoechst 33342 and NPN uptake assays of strains reveal loss of *ogcA* and *ogcX* leads to increased fluorescence upon induction, supporting enhanced membrane permeability (n=6 for Hoechst 33342, n=5 for NPN). The fluorescence intensities have been normalised against bacterial cell counts.

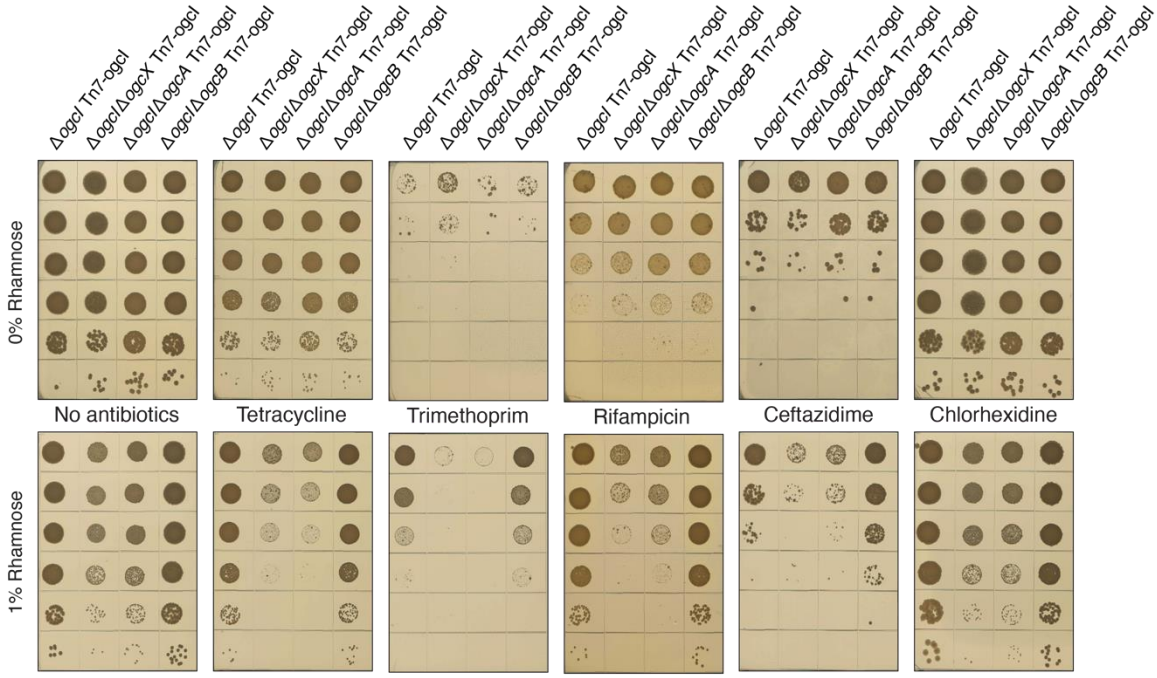

Figure 6. Loss of *ogcA* and *ogcX* sensitise *B. cenocepacia* to antimicrobials. Spot plate assays of *B. cenocepacia* strains, including Δ*ogcI* Tn7-*ogcI*, Δ*ogcI*Δ*ogcX* Tn7-*ogcI*, Δ*ogcI*Δ*ogcA* Tn7-*ogcI*, and Δ*ogcI*Δ*ogcB* Tn7-*ogcI* on CAMHA containing various antibiotics, with or without induction with 1% rhamnose. Rhamnose-induced glycosylation resulted in increased susceptibility to tetracycline, rifampicin, trimethoprim and ceftazidime in strains lacking *ogcA* and *ogcX*. Data representative of four biological replicates per strain per antimicrobial.

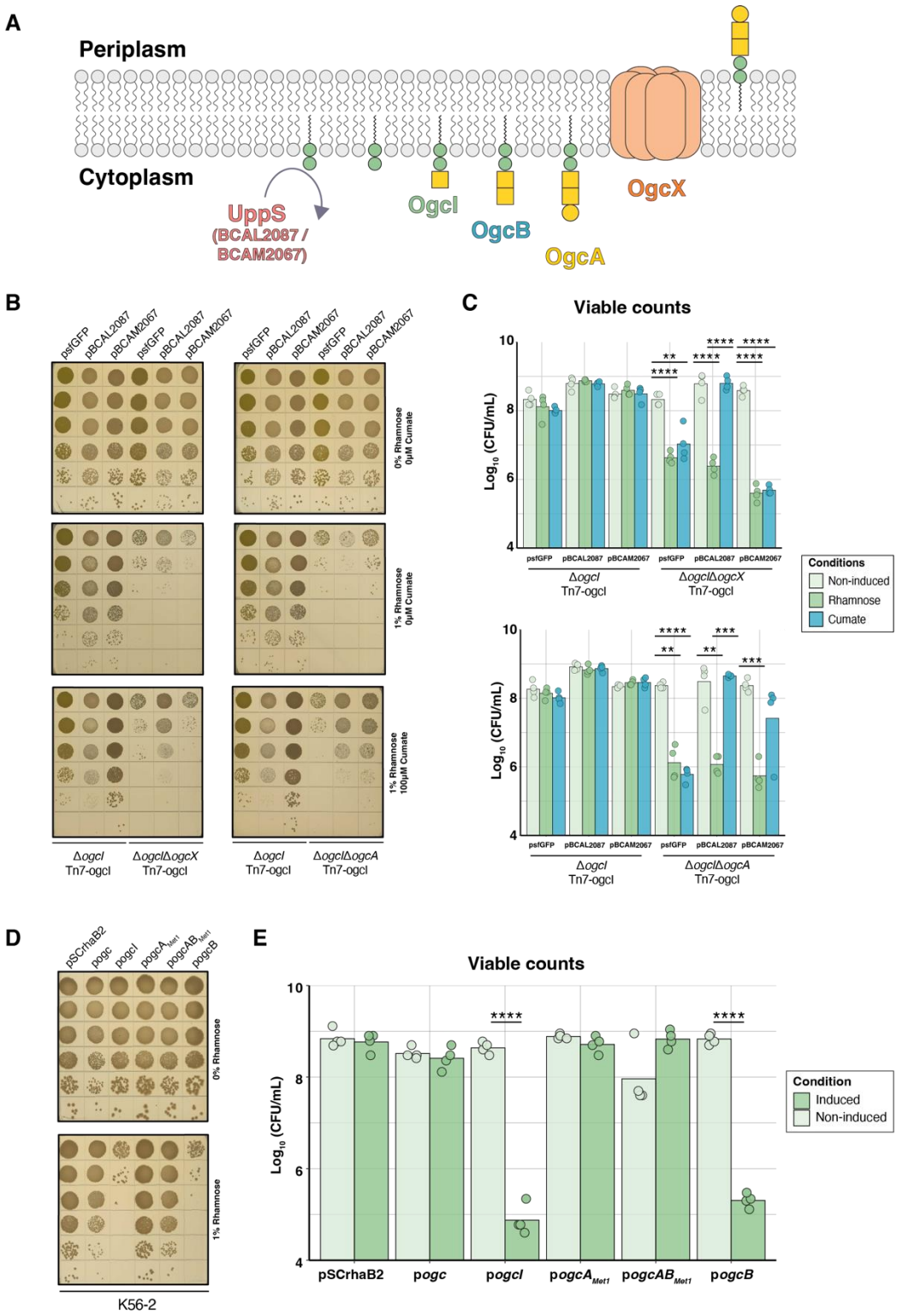

Figure 7. Modulation of upstream and early steps in *ogc* biosynthesis impacts *B. cenocepacia* viability. A) Proposed enzymes responsible for the *de novo* synthesis of the undecaprenyl pool and early steps in *ogc* biosynthesis**.** Within *B. cenocepacia*, two putative undecaprenyl pyrophosphate synthases (UppS) are assigned corresponding to BCAL2087 and BCAM2067, while OgcI is responsible for *OGC* initiation and OgcB the addition of the second

GalNAc[46]. **B-C)** Spot plate assays and viable counts of the *B. cenocepacia* Δ*ogcI* Tn7-*ogcI*, Δ*ogcI*Δ*ogcX* Tn7-*ogcI* and Δ*ogcI*Δ*ogcA* Tn7-*ogcI* containing pcumate-sfGFP, pcumate-BCAL2087 or pcumate-BCAM2067 reveal the initiation of glycosylation reduces viability while induction of putative UppS partially restores the defect observed within Δ*ogcA* and Δ*ogcX* strains. **D-E)** Spot plate assays of *B. cenocepacia* K56-2 (WT) containing the expression vectors pSCrhaB2, pSCrhaB2-*ogc (*p*ogc)*, pSCrhaB2-*ogcI (*p*ogcI)*, pSCrhaB2-*ogcA-Met1 (*p*ogcA*$_{\text{Met1}}$), pSCrhaB2-*ogcB* (p*ogcB*), pSCrhaB2-*ogcAB-Met1* (p*ogcAB*$_{\text{Met1}}$). Induction of *ogc*I and *ogc*B results in reduced viability, while the expression of *ogc*A and *ogcAB* demonstrated no reduction in viability.

References:

1 Touz, E. T. & Mengin-Lecreulx, D. Undecaprenyl Phosphate Synthesis. *EcoSal Plus* **3** (2008). https://doi.org:10.1128/ecosalplus.4.7.1.7

2 Workman, S. D. & Strynadka, N. C. J. A Slippery Scaffold: Synthesis and Recycling of the Bacterial Cell Wall Carrier Lipid. *J Mol Biol* **432**, 4964-4982 (2020). https://doi.org:10.1016/j.jmb.2020.03.025

3 Hong, Y., Cunneen, M. M. & Reeves, P. R. The Wzx translocases for Salmonella enterica O-antigen processing have unexpected serotype specificity. *Molecular microbiology* **84**, 620-630 (2012). https://doi.org:10.1111/j.1365-2958.2012.08048.x

4 Liu, M. A., Stent, T. L., Hong, Y. & Reeves, P. R. Inefficient translocation of a truncated O unit by a Salmonella Wzx affects both O-antigen production and cell growth. *FEMS Microbiol Lett* **362** (2015). https://doi.org:10.1093/femsle/fnv053

5 Barreteau, H. *et al.* Quantitative high-performance liquid chromatography analysis of the pool levels of undecaprenyl phosphate and its derivatives in bacterial membranes. *J Chromatogr B Analyt Technol Biomed Life Sci* **877**, 213-220 (2009). https://doi.org:10.1016/j.jchromb.2008.12.010

6 Jorgenson, M. A. & Young, K. D. Interrupting biosynthesis of O-antigen or the lipopolysaccharide core produces morphological defects in Escherichia coli by sequestering undecaprenyl phosphate. *Journal of bacteriology* (2016). https://doi.org:10.1128/JB.00550-16

7 Jorgenson, M. A., Kannan, S., Laubacher, M. E. & Young, K. D. Dead-end intermediates in the enterobacterial common antigen pathway induce morphological defects in Escherichia coli by competing for undecaprenyl phosphate. *Molecular microbiology* **100**, 1-14 (2016). https://doi.org:10.1111/mmi.13284

8 Tatar, L. D., Marolda, C. L., Polischuk, A. N., van Leeuwen, D. & Valvano, M. A. An Escherichia coli undecaprenyl-pyrophosphate phosphatase implicated in undecaprenyl phosphate recycling. *Microbiology (Reading)* **153**, 2518-2529 (2007). https://doi.org:10.1099/mic.0.2007/006312-0

9 Yuasa, R., Levinthal, M. & Nikaido, H. Biosynthesis of cell wall lipopolysaccharide in mutants of Salmonella. V. A mutant of Salmonella typhimurium defective in the synthesis of cytidine diphosphoabequose. *Journal of bacteriology* **100**, 433-444 (1969). https://doi.org:10.1128/jb.100.1.433-444.1969

10 Rick, P. D. *et al.* Evidence that the wzxE gene of Escherichia coli K-12 encodes a protein involved in the transbilayer movement of a trisaccharide-lipid intermediate in the assembly of enterobacterial common antigen. *The Journal of biological chemistry* **278**, 16534-16542 (2003). https://doi.org:10.1074/jbc.M301750200

11 Qin, J., Hong, Y. & Totsika, M. Determining glycosyltransferase functional order via lethality due to accumulated O-antigen intermediates, exemplified with Shigella flexneri O-antigen biosynthesis. *Applied and environmental microbiology* **90**, e0220323 (2024). https://doi.org:10.1128/aem.02203-23

12 Swoboda, J. G. *et al.* Discovery of a small molecule that blocks wall teichoic acid biosynthesis in Staphylococcus aureus. *ACS Chem Biol* **4**, 875-883 (2009). https://doi.org:10.1021/cb900151k

13 Muscato, J. D. *et al.* Rapid Inhibitor Discovery by Exploiting Synthetic Lethality. *J Am Chem Soc* **144**, 3696-3705 (2022). https://doi.org:10.1021/jacs.1c12697

14 Sham, L. T., Zheng, S., Yakhnina, A. A., Kruse, A. C. & Bernhardt, T. G. Loss of specificity variants of WzxC suggest that substrate recognition is coupled with transporter opening in MOP-family flippases. *Molecular microbiology* **109**, 633-641 (2018). https://doi.org:10.1111/mmi.14002

15 Chua, W. Z. *et al.* High-Throughput Mutagenesis and Cross-Complementation Experiments Reveal Substrate Preference and Critical Residues of the Capsule Transporters in Streptococcus pneumoniae. *mBio* **12**, e0261521 (2021). https://doi.org:10.1128/mBio.02615-21
16 Su, T. *et al.* Rewiring the pneumococcal capsule pathway for investigating glycosyltransferase specificity and genetic glycoengineering. *Sci Adv* **9**, eadi8157 (2023). https://doi.org:10.1126/sciadv.adi8157
17 Ruiz, N. Lipid Flippases for Bacterial Peptidoglycan Biosynthesis. *Lipid Insights* **8**, 21-31 (2015). https://doi.org:10.4137/LPI.S31783
18 Cuthbertson, L., Kos, V. & Whitfield, C. ABC transporters involved in export of cell surface glycoconjugates. *Microbiol Mol Biol Rev* **74**, 341-362 (2010). https://doi.org:10.1128/MMBR.00009-10
19 Kuk, A. C. Y., Hao, A. & Lee, S. Y. Structure and Mechanism of the Lipid Flippase MurJ. *Annu Rev Biochem* **91**, 705-729 (2022). https://doi.org:10.1146/annurev-biochem-040320-105145
20 Hong, Y., Liu, M. A. & Reeves, P. R. Progress in Our Understanding of Wzx Flippase for Translocation of Bacterial Membrane Lipid-Linked Oligosaccharide. *Journal of bacteriology* **200** (2018). https://doi.org:10.1128/JB.00154-17
21 Liu, D., Cole, R. A. & Reeves, P. R. An O-antigen processing function for Wzx (RfbX): a promising candidate for O-unit flippase. *Journal of bacteriology* **178**, 2102-2107 (1996). https://doi.org:10.1128/jb.178.7.2102-2107.1996
22 Kenyon, J. J. & Hall, R. M. Variation in the complex carbohydrate biosynthesis loci of Acinetobacter baumannii genomes. *PloS one* **8**, e62160 (2013). https://doi.org:10.1371/journal.pone.0062160
23 Paton, J. C. & Trappetti, C. Streptococcus pneumoniae Capsular Polysaccharide. *Microbiol Spectr* **7** (2019). https://doi.org:10.1128/microbiolspec.GPP3-0019-2018
24 Becker, A. Challenges and perspectives in combinatorial assembly of novel exopolysaccharide biosynthesis pathways. *Front Microbiol* **6**, 687 (2015). https://doi.org:10.3389/fmicb.2015.00687
25 Feldman, M. F. *et al.* The activity of a putative polyisoprenol-linked sugar translocase (Wzx) involved in Escherichia coli O antigen assembly is independent of the chemical structure of the O repeat. *The Journal of biological chemistry* **274**, 35129-35138 (1999).
26 Marolda, C. L., Vicarioli, J. & Valvano, M. A. Wzx proteins involved in biosynthesis of O antigen function in association with the first sugar of the O-specific lipopolysaccharide subunit. *Microbiology (Reading)* **150**, 4095-4105 (2004). https://doi.org:10.1099/mic.0.27456-0
27 Hong, Y. & Reeves, P. R. Diversity of o-antigen repeat unit structures can account for the substantial sequence variation of wzx translocases. *Journal of bacteriology* **196**, 1713-1722 (2014). https://doi.org:10.1128/JB.01323-13
28 Liu, D. & Reeves, P. R. Escherichia coli K12 regains its O antigen. *Microbiology (Reading)* **140 (Pt 1)**, 49-57 (1994). https://doi.org:10.1099/13500872-140-1-49
29 Stevenson, G. *et al.* Structure of the O antigen of Escherichia coli K-12 and the sequence of its rfb gene cluster. *Journal of bacteriology* **176**, 4144-4156 (1994). https://doi.org:10.1128/jb.176.13.4144-4156.1994
30 Barr, K. & Rick, P. D. Biosynthesis of enterobacterial common antigen in Escherichia coli. In vitro synthesis of lipid-linked intermediates. *The Journal of biological chemistry* **262**, 7142-7150 (1987).
31 Barr, K., Ward, S., Meier-Dieter, U., Mayer, H. & Rick, P. D. Characterization of an Escherichia coli rff mutant defective in transfer of N-acetylmannosaminuronic acid

(ManNAcA) from UDP-ManNAcA to a lipid-linked intermediate involved in enterobacterial common antigen synthesis. *Journal of bacteriology* **170**, 228-233 (1988). https://doi.org:10.1128/jb.170.1.228-233.1988

32 Burrows, L. L. & Lam, J. S. Effect of wzx (rfbX) mutations on A-band and B-band lipopolysaccharide biosynthesis in Pseudomonas aeruginosa O5. *Journal of bacteriology* **181**, 973-980 (1999). https://doi.org:10.1128/JB.181.3.973-980.1999

33 Xayarath, B. & Yother, J. Mutations blocking side chain assembly, polymerization, or transport of a Wzy-dependent Streptococcus pneumoniae capsule are lethal in the absence of suppressor mutations and can affect polymer transfer to the cell wall. *Journal of bacteriology* **189**, 3369-3381 (2007). https://doi.org:10.1128/JB.01938-06

34 Bai, J. *et al.* Essential Gene Analysis in Acinetobacter baumannii by High-Density Transposon Mutagenesis and CRISPR Interference. *Journal of bacteriology* **203**, e0056520 (2021). https://doi.org:10.1128/JB.00565-20

35 Koomey, M. O-linked protein glycosylation in bacteria: snapshots and current perspectives. *Curr Opin Struct Biol* **56**, 198-203 (2019). https://doi.org:10.1016/j.sbi.2019.03.020

36 Nothaft, H. & Szymanski, C. M. Protein glycosylation in bacteria: sweeter than ever. *Nature reviews. Microbiology* **8**, 765-778 (2010). https://doi.org:10.1038/nrmicro2383

37 Nothaft, H. *et al.* Diversity in the protein N-glycosylation pathways within the Campylobacter genus. *Molecular & cellular proteomics : MCP* **11**, 1203-1219 (2012). https://doi.org:10.1074/mcp.M112.021519

38 Jervis, A. J. *et al.* Characterization of the structurally diverse N-linked glycans of Campylobacter species. *Journal of bacteriology* **194**, 2355-2362 (2012). https://doi.org:10.1128/JB.00042-12

39 Hadjineophytou, C. *et al.* Genetic determinants of genus-Level glycan diversity in a bacterial protein glycosylation system. *PLoS Genet* **15**, e1008532 (2019). https://doi.org:10.1371/journal.pgen.1008532

40 Anonsen, J. H. *et al.* Characterization of a Unique Tetrasaccharide and Distinct Glycoproteome in the O-Linked Protein Glycosylation System of Neisseria elongata subsp. glycolytica. *Journal of bacteriology* **198**, 256-267 (2016). https://doi.org:10.1128/JB.00620-15

41 Vik, A. *et al.* Broad spectrum O-linked protein glycosylation in the human pathogen Neisseria gonorrhoeae. *Proceedings of the National Academy of Sciences of the United States of America* **106**, 4447-4452 (2009). https://doi.org:10.1073/pnas.0809504106

42 Borud, B. *et al.* Genetic, structural, and antigenic analyses of glycan diversity in the O-linked protein glycosylation systems of human Neisseria species. *Journal of bacteriology* **192**, 2816-2829 (2010). https://doi.org:10.1128/JB.00101-10

43 Hadjineophytou, C. *et al.* Sculpting the Bacterial O-Glycoproteome: Functional Analyses of Orthologous Oligosaccharyltransferases with Diverse Targeting Specificities. *mBio*, e0379721 (2022). https://doi.org:10.1128/mbio.03797-21

44 Hayes, A. J., Lewis, J. M., Davies, M. R. & Scott, N. E. Burkholderia PglL enzymes are Serine preferring oligosaccharyltransferases which target conserved proteins across the Burkholderia genus. *Commun Biol* **4**, 1045 (2021). https://doi.org:10.1038/s42003-021-02588-y

45 Ahmad Izaham, A. R. & Scott, N. E. Open Database Searching Enables the Identification and Comparison of Bacterial Glycoproteomes without Defining Glycan Compositions Prior to Searching. *Molecular & cellular proteomics : MCP* **19**, 1561-1574 (2020). https://doi.org:10.1074/mcp.TIR120.002100

46 Fathy Mohamed, Y. *et al.* A general protein O-glycosylation machinery conserved in Burkholderia species improves bacterial fitness and elicits glycan immunogenicity in humans. *The Journal of biological chemistry* **294**, 13248-13268 (2019). https://doi.org:10.1074/jbc.RA119.009671
47 Iwashkiw, J. A., Vozza, N. F., Kinsella, R. L. & Feldman, M. F. Pour some sugar on it: the expanding world of bacterial protein O-linked glycosylation. *Molecular microbiology* **89**, 14-28 (2013). https://doi.org:10.1111/mmi.12265
48 Nothaft, H. & Szymanski, C. M. New discoveries in bacterial N-glycosylation to expand the synthetic biology toolbox. *Curr Opin Chem Biol* **53**, 16-24 (2019). https://doi.org:10.1016/j.cbpa.2019.05.032
49 Borud, B. & Koomey, M. Sweet complexity: O-linked protein glycosylation in pathogenic Neisseria. *Frontiers in cellular and infection microbiology* **14**, 1407863 (2024). https://doi.org:10.3389/fcimb.2024.1407863
50 Linton, D. *et al.* Functional analysis of the Campylobacter jejuni N-linked protein glycosylation pathway. *Molecular microbiology* **55**, 1695-1703 (2005). https://doi.org:10.1111/j.1365-2958.2005.04519.x
51 Perez, C. *et al.* Structure and mechanism of an active lipid-linked oligosaccharide flippase. *Nature* **524**, 433-438 (2015). https://doi.org:10.1038/nature14953
52 Alaimo, C. *et al.* Two distinct but interchangeable mechanisms for flipping of lipid-linked oligosaccharides. *EMBO J* **25**, 967-976 (2006). https://doi.org:10.1038/sj.emboj.7601024
53 Kahler, C. M. *et al.* Polymorphisms in pilin glycosylation Locus of Neisseria meningitidis expressing class II pili. *Infection and immunity* **69**, 3597-3604 (2001). https://doi.org:10.1128/IAI.69.6.3597-3604.2001
54 Power, P. M. *et al.* Genetic characterization of pilin glycosylation in Neisseria meningitidis. *Microbiology* **146 (Pt 4)**, 967-979 (2000). https://doi.org:10.1099/00221287-146-4-967
55 Aas, F. E., Vik, A., Vedde, J., Koomey, M. & Egge-Jacobsen, W. Neisseria gonorrhoeae O-linked pilin glycosylation: functional analyses define both the biosynthetic pathway and glycan structure. *Molecular microbiology* **65**, 607-624 (2007). https://doi.org:10.1111/j.1365-2958.2007.05806.x
56 Johannessen, C., Koomey, M. & Borud, B. Hypomorphic glycosyltransferase alleles and recoding at contingency loci influence glycan microheterogeneity in the protein glycosylation system of Neisseria species. *Journal of bacteriology* **194**, 5034-5043 (2012). https://doi.org:10.1128/JB.00950-12
57 Wang, N. *et al.* Allelic polymorphisms in a glycosyltransferase gene shape glycan repertoire in the O-linked protein glycosylation system of Neisseria. *Glycobiology* **31**, 477-491 (2021). https://doi.org:10.1093/glycob/cwaa073
58 Lithgow, K. V. *et al.* A general protein O-glycosylation system within the Burkholderia cepacia complex is involved in motility and virulence. *Molecular microbiology* **92**, 116-137 (2014). https://doi.org:10.1111/mmi.12540
59 Gislason, A. S., Turner, K., Domaratzki, M. & Cardona, S. T. Comparative analysis of the Burkholderia cenocepacia K56-2 essential genome reveals cell envelope functions that are uniquely required for survival in species of the genus Burkholderia. *Microb Genom* **3** (2017). https://doi.org:10.1099/mgen.0.000140
60 Hogan, A. M. *et al.* Profiling cell envelope-antibiotic interactions reveals vulnerabilities to beta-lactams in a multidrug-resistant bacterium. *Nat Commun* **14**, 4815 (2023). https://doi.org:10.1038/s41467-023-40494-5

61 Moule, M. G. *et al.* Genome-wide saturation mutagenesis of Burkholderia pseudomallei K96243 predicts essential genes and novel targets for antimicrobial development. *MBio* **5**, e00926-00913 (2014). https://doi.org:10.1128/mBio.00926-13
62 Oppy, C. C. *et al.* Loss of O-linked protein glycosylation in Burkholderia cenocepacia impairs biofilm formation, siderophore activity and alters transcriptional regulators *mSphere* **4**, e00660-00619 (2019).
63 Cardona, S. T. & Valvano, M. A. An expression vector containing a rhamnose-inducible promoter provides tightly regulated gene expression in Burkholderia cenocepacia. *Plasmid* **54**, 219-228 (2005). https://doi.org:10.1016/j.plasmid.2005.03.004
64 Lopez, C. M., Rholl, D. A., Trunck, L. A. & Schweizer, H. P. Versatile dual-technology system for markerless allele replacement in Burkholderia pseudomallei. *Applied and environmental microbiology* **75**, 6496-6503 (2009). https://doi.org:10.1128/AEM.01669-09
65 Aubert, D. F., Hamad, M. A. & Valvano, M. A. A markerless deletion method for genetic manipulation of Burkholderia cenocepacia and other multidrug-resistant gram-negative bacteria. *Methods in molecular biology* **1197**, 311-327 (2014). https://doi.org:10.1007/978-1-4939-1261-2_18
66 Garcia, E. C., Anderson, M. S., Hagar, J. A. & Cotter, P. A. Burkholderia BcpA mediates biofilm formation independently of interbacterial contact-dependent growth inhibition. *Molecular microbiology* **89**, 1213-1225 (2013). https://doi.org:10.1111/mmi.12339
67 Flannagan, R. S., Linn, T. & Valvano, M. A. A system for the construction of targeted unmarked gene deletions in the genus Burkholderia. *Environ Microbiol* **10**, 1652-1660 (2008). https://doi.org:10.1111/j.1462-2920.2008.01576.x
68 Gibson, D. G. *et al.* Enzymatic assembly of DNA molecules up to several hundred kilobases. *Nature methods* **6**, 343-345 (2009). https://doi.org:10.1038/nmeth.1318
69 Lefebre, M. D. & Valvano, M. A. Construction and evaluation of plasmid vectors optimized for constitutive and regulated gene expression in Burkholderia cepacia complex isolates. *Applied and environmental microbiology* **68**, 5956-5964 (2002).
70 Sambrook, J., E. F. Fritsch, and T. Maniatis. *Molecular cloning: a laboratory manual*. (Cold Spring Harbor Laboratory, Cold Spring Harbor, 1990).
71 Figurski, D. H. & Helinski, D. R. Replication of an origin-containing derivative of plasmid RK2 dependent on a plasmid function provided in trans. *Proceedings of the National Academy of Sciences of the United States of America* **76**, 1648-1652 (1979). https://doi.org:10.1073/pnas.76.4.1648
72 Choi, K. H., DeShazer, D. & Schweizer, H. P. mini-Tn7 insertion in bacteria with multiple glmS-linked attTn7 sites: example Burkholderia mallei ATCC 23344. *Nature protocols* **1**, 162-169 (2006). https://doi.org:10.1038/nprot.2006.25
73 Hamad, M. A., Di Lorenzo, F., Molinaro, A. & Valvano, M. A. Aminoarabinose is essential for lipopolysaccharide export and intrinsic antimicrobial peptide resistance in Burkholderia cenocepacia(dagger). *Molecular microbiology* **85**, 962-974 (2012). https://doi.org:10.1111/j.1365-2958.2012.08154.x
74 Bernier, S. P., Son, S. & Surette, M. G. The Mla Pathway Plays an Essential Role in the Intrinsic Resistance of Burkholderia cepacia Complex Species to Antimicrobials and Host Innate Components. *Journal of bacteriology* **200** (2018). https://doi.org:10.1128/JB.00156-18
75 Malinverni, J. C. & Silhavy, T. J. An ABC transport system that maintains lipid asymmetry in the gram-negative outer membrane. *Proceedings of the National*

Academy of Sciences of the United States of America **106**, 8009-8014 (2009). https://doi.org:10.1073/pnas.0903229106
76 Mychack, A. *et al.* A synergistic role for two predicted inner membrane proteins of Escherichia coli in cell envelope integrity. *Molecular microbiology* **111**, 317-337 (2019). https://doi.org:10.1111/mmi.14157
77 Schindelin, J. *et al.* Fiji: an open-source platform for biological-image analysis. *Nature methods* **9**, 676-682 (2012). https://doi.org:10.1038/nmeth.2019
78 Jassem, A. N. *et al.* In vitro susceptibility of Burkholderia vietnamiensis to aminoglycosides. *Antimicrobial agents and chemotherapy* **55**, 2256-2264 (2011). https://doi.org:10.1128/AAC.01434-10
79 Richmond, G. E., Chua, K. L. & Piddock, L. J. Efflux in Acinetobacter baumannii can be determined by measuring accumulation of H33342 (bis-benzamide). *J Antimicrob Chemother* **68**, 1594-1600 (2013). https://doi.org:10.1093/jac/dkt052
80 Krishnamoorthy, G. *et al.* Efflux Pumps of Burkholderia thailandensis Control the Permeability Barrier of the Outer Membrane. *Antimicrobial agents and chemotherapy* **63** (2019). https://doi.org:10.1128/AAC.00956-19
81 Helander, I. M. & Mattila-Sandholm, T. Fluorometric assessment of gram-negative bacterial permeabilization. *J Appl Microbiol* **88**, 213-219 (2000). https://doi.org:10.1046/j.1365-2672.2000.00971.x
82 Loh, B., Grant, C. & Hancock, R. E. Use of the fluorescent probe 1-N-phenylnaphthylamine to study the interactions of aminoglycoside antibiotics with the outer membrane of Pseudomonas aeruginosa. *Antimicrobial agents and chemotherapy* **26**, 546-551 (1984). https://doi.org:10.1128/AAC.26.4.546
83 Malott, R. J., Steen-Kinnaird, B. R., Lee, T. D. & Speert, D. P. Identification of hopanoid biosynthesis genes involved in polymyxin resistance in Burkholderia multivorans. *Antimicrobial agents and chemotherapy* **56**, 464-471 (2012). https://doi.org:10.1128/AAC.00602-11
84 Kulak, N. A., Pichler, G., Paron, I., Nagaraj, N. & Mann, M. Minimal, encapsulated proteomic-sample processing applied to copy-number estimation in eukaryotic cells. *Nature methods* **11**, 319-324 (2014). https://doi.org:10.1038/nmeth.2834
85 Harney, D. J. *et al.* Proteomic Analysis of Human Plasma during Intermittent Fasting. *Journal of proteome research* **18**, 2228-2240 (2019). https://doi.org:10.1021/acs.jproteome.9b00090
86 Rappsilber, J., Mann, M. & Ishihama, Y. Protocol for micro-purification, enrichment, pre-fractionation and storage of peptides for proteomics using StageTips. *Nature protocols* **2**, 1896-1906 (2007). https://doi.org:10.1038/nprot.2007.261
87 Ahmad Izaham, A. R. *et al.* What Are We Missing by Using Hydrophilic Enrichment? Improving Bacterial Glycoproteome Coverage Using Total Proteome and FAIMS Analyses. *Journal of proteome research* **20**, 599-612 (2021). https://doi.org:10.1021/acs.jproteome.0c00565
88 Saba, J., Dutta, S., Hemenway, E. & Viner, R. Increasing the productivity of glycopeptides analysis by using higher-energy collision dissociation-accurate mass-product-dependent electron transfer dissociation. *Int J Proteomics* **2012**, 560391 (2012). https://doi.org:10.1155/2012/560391
89 Caval, T., Zhu, J. & Heck, A. J. R. Simply Extending the Mass Range in Electron Transfer Higher Energy Collisional Dissociation Increases Confidence in N-Glycopeptide Identification. *Anal Chem* **91**, 10401-10406 (2019). https://doi.org:10.1021/acs.analchem.9b02125
90 Polasky, D. A., Geiszler, D. J., Yu, F. & Nesvizhskii, A. I. Multi-attribute Glycan Identification and FDR Control for Glycoproteomics. *Molecular & cellular*

proteomics : MCP, 100205 (2022). https://doi.org:https://doi.org/10.1016/j.mcpro.2022.100205

91 Kong, A. T., Leprevost, F. V., Avtonomov, D. M., Mellacheruvu, D. & Nesvizhskii, A. I. MSFragger: ultrafast and comprehensive peptide identification in mass spectrometry-based proteomics. *Nature methods* **14**, 513-520 (2017). https://doi.org:10.1038/nmeth.4256

92 Polasky, D. A., Yu, F., Teo, G. C. & Nesvizhskii, A. I. Fast and comprehensive N- and O-glycoproteomics analysis with MSFragger-Glyco. *Nature methods* **17**, 1125-1132 (2020). https://doi.org:10.1038/s41592-020-0967-9

93 Holden, M. T. *et al.* The genome of Burkholderia cenocepacia J2315, an epidemic pathogen of cystic fibrosis patients. *Journal of bacteriology* **191**, 261-277 (2009). https://doi.org:10.1128/JB.01230-08

94 Cox, J. *et al.* Accurate proteome-wide label-free quantification by delayed normalization and maximal peptide ratio extraction, termed MaxLFQ. *Molecular & cellular proteomics : MCP* **13**, 2513-2526 (2014). https://doi.org:10.1074/mcp.M113.031591

95 Tyanova, S. *et al.* The Perseus computational platform for comprehensive analysis of (prote)omics data. *Nature methods* **13**, 731-740 (2016). https://doi.org:10.1038/nmeth.3901

96 Wickham, H. *ggplot2: Elegant Graphics for Data Analysis*. (Springer-Verlag New York, 2016).

97 Varga, J. J. *et al.* Draft Genome Sequences of Burkholderia cenocepacia ET12 Lineage Strains K56-2 and BC7. *Genome Announc* **1** (2013). https://doi.org:10.1128/genomeA.00841-13

98 Perez-Riverol, Y. *et al.* The PRIDE database and related tools and resources in 2019: improving support for quantification data. *Nucleic Acids Res* **47**, D442-D450 (2019). https://doi.org:10.1093/nar/gky1106

99 Vizcaino, J. A. *et al.* 2016 update of the PRIDE database and its related tools. *Nucleic Acids Res* **44**, D447-456 (2016). https://doi.org:10.1093/nar/gkv1145

100 Ludwig, C. *et al.* Data-independent acquisition-based SWATH-MS for quantitative proteomics: a tutorial. *Mol Syst Biol* **14**, e8126 (2018). https://doi.org:10.15252/msb.20178126

101 Pino, L. K., Just, S. C., MacCoss, M. J. & Searle, B. C. Acquiring and Analyzing Data Independent Acquisition Proteomics Experiments without Spectrum Libraries. *Molecular & cellular proteomics : MCP* **19**, 1088-1103 (2020). https://doi.org:10.1074/mcp.P119.001913

102 Mitchell, A. M., Srikumar, T. & Silhavy, T. J. Cyclic Enterobacterial Common Antigen Maintains the Outer Membrane Permeability Barrier of Escherichia coli in a Manner Controlled by YhdP. *mBio* **9** (2018). https://doi.org:10.1128/mBio.01321-18

103 Jorgenson, M. A. *et al.* Simultaneously inhibiting undecaprenyl phosphate production and peptidoglycan synthases promotes rapid lysis in Escherichia coli. *Molecular microbiology* **112**, 233-248 (2019). https://doi.org:10.1111/mmi.14265

104 Lewis, J. M. & Scott, N. E. CRISPRi-Mediated Silencing of Burkholderia O-Linked Glycosylation Systems Enables the Depletion of Glycosylation Yet Results in Modest Proteome Impacts. *Journal of proteome research* **22**, 1762-1778 (2023). https://doi.org:10.1021/acs.jproteome.2c00790

105 Lewis, J. M., Jebeli, L., Coulon, P. M. L., Lay, C. E. & Scott, N. E. Glycoproteomic and proteomic analysis of Burkholderia cenocepacia reveals glycosylation events within FliF and MotB are dispensable for motility. *Microbiol Spectr* **12**, e0034624 (2024). https://doi.org:10.1128/spectrum.00346-24

106 Tkalec, K. I. *et al.* Glycan-Tailored Glycoproteomic Analysis Reveals Serine is the Sole Residue Subjected to O-Linked Glycosylation in Acinetobacter baumannii. *Journal of proteome research* **23**, 2474-2494 (2024). https://doi.org:10.1021/acs.jproteome.4c00148
107 Scott, N. E. *et al.* Diversity within the O-linked protein glycosylation systems of acinetobacter species. *Molecular & cellular proteomics : MCP* **13**, 2354-2370 (2014). https://doi.org:10.1074/mcp.M114.038315
108 Iwashkiw, J. A. *et al.* Identification of a general O-linked protein glycosylation system in Acinetobacter baumannii and its role in virulence and biofilm formation. *PLoS pathogens* **8**, e1002758 (2012). https://doi.org:10.1371/journal.ppat.1002758
109 Naess, L. M. *et al.* Genetic, Functional, and Immunogenic Analyses of the O-Linked Protein Glycosylation System in Neisseria meningitidis Serogroup A ST-7 Isolates. *Journal of bacteriology* **205**, e0045822 (2023). https://doi.org:10.1128/jb.00458-22
110 Kuhn, H. M., Meier-Dieter, U. & Mayer, H. ECA, the enterobacterial common antigen. *FEMS microbiology reviews* **4**, 195-222 (1988). https://doi.org:10.1111/j.1574-6968.1988.tb02743.x
111 Rai, A. K. & Mitchell, A. M. Enterobacterial Common Antigen: Synthesis and Function of an Enigmatic Molecule. *mBio* **11** (2020). https://doi.org:10.1128/mBio.01914-20
112 Kajimura, J., Rahman, A. & Rick, P. D. Assembly of cyclic enterobacterial common antigen in Escherichia coli K-12. *Journal of bacteriology* **187**, 6917-6927 (2005). https://doi.org:10.1128/JB.187.20.6917-6927.2005
113 Mohamed, Y. F. & Valvano, M. A. A Burkholderia cenocepacia MurJ (MviN) homolog is essential for cell wall peptidoglycan synthesis and bacterial viability. *Glycobiology* **24**, 564-576 (2014). https://doi.org:10.1093/glycob/cwu025
114 Cain, A. K. *et al.* A decade of advances in transposon-insertion sequencing. *Nat Rev Genet* **21**, 526-540 (2020). https://doi.org:10.1038/s41576-020-0244-x
115 Mateus, A. *et al.* Transcriptional and Post-Transcriptional Polar Effects in Bacterial Gene Deletion Libraries. *mSystems* **6**, e0081321 (2021). https://doi.org:10.1128/mSystems.00813-21
116 Hutchison, C. A., 3rd *et al.* Polar Effects of Transposon Insertion into a Minimal Bacterial Genome. *Journal of bacteriology* **201** (2019). https://doi.org:10.1128/JB.00185-19
117 Sass, A., Everaert, A., Van Acker, H., Van den Driessche, F. & Coenye, T. Targeting the Nonmevalonate Pathway in Burkholderia cenocepacia Increases Susceptibility to Certain beta-Lactam Antibiotics. *Antimicrobial agents and chemotherapy* **62** (2018). https://doi.org:10.1128/AAC.02607-17
118 Zhao, L., Chang, W. C., Xiao, Y., Liu, H. W. & Liu, P. Methylerythritol phosphate pathway of isoprenoid biosynthesis. *Annu Rev Biochem* **82**, 497-530 (2013). https://doi.org:10.1146/annurev-biochem-052010-100934
119 Eade, C. R. *et al.* Making the Enterobacterial Common Antigen Glycan and Measuring Its Substrate Sequestration. *ACS Chem Biol* **16**, 691-700 (2021). https://doi.org:10.1021/acschembio.0c00983
120 Horzempa, J., Dean, C. R., Goldberg, J. B. & Castric, P. Pseudomonas aeruginosa 1244 pilin glycosylation: glycan substrate recognition. *Journal of bacteriology* **188**, 4244-4252 (2006). https://doi.org:10.1128/JB.00273-06
121 Castric, P., Cassels, F. J. & Carlson, R. W. Structural characterization of the Pseudomonas aeruginosa 1244 pilin glycan. *The Journal of biological chemistry* **276**, 26479-26485 (2001). https://doi.org:10.1074/jbc.M102685200

122 Lees-Miller, R. G. *et al.* A common pathway for O-linked protein-glycosylation and synthesis of capsule in Acinetobacter baumannii. *Molecular microbiology* **89**, 816-830 (2013). https://doi.org:10.1111/mmi.12300

123 Knoot, C. J. *et al.* Discovery and characterization of a new class of O-linking oligosaccharyltransferases from the Moraxellaceae family. *Glycobiology* (2022). https://doi.org:10.1093/glycob/cwac070

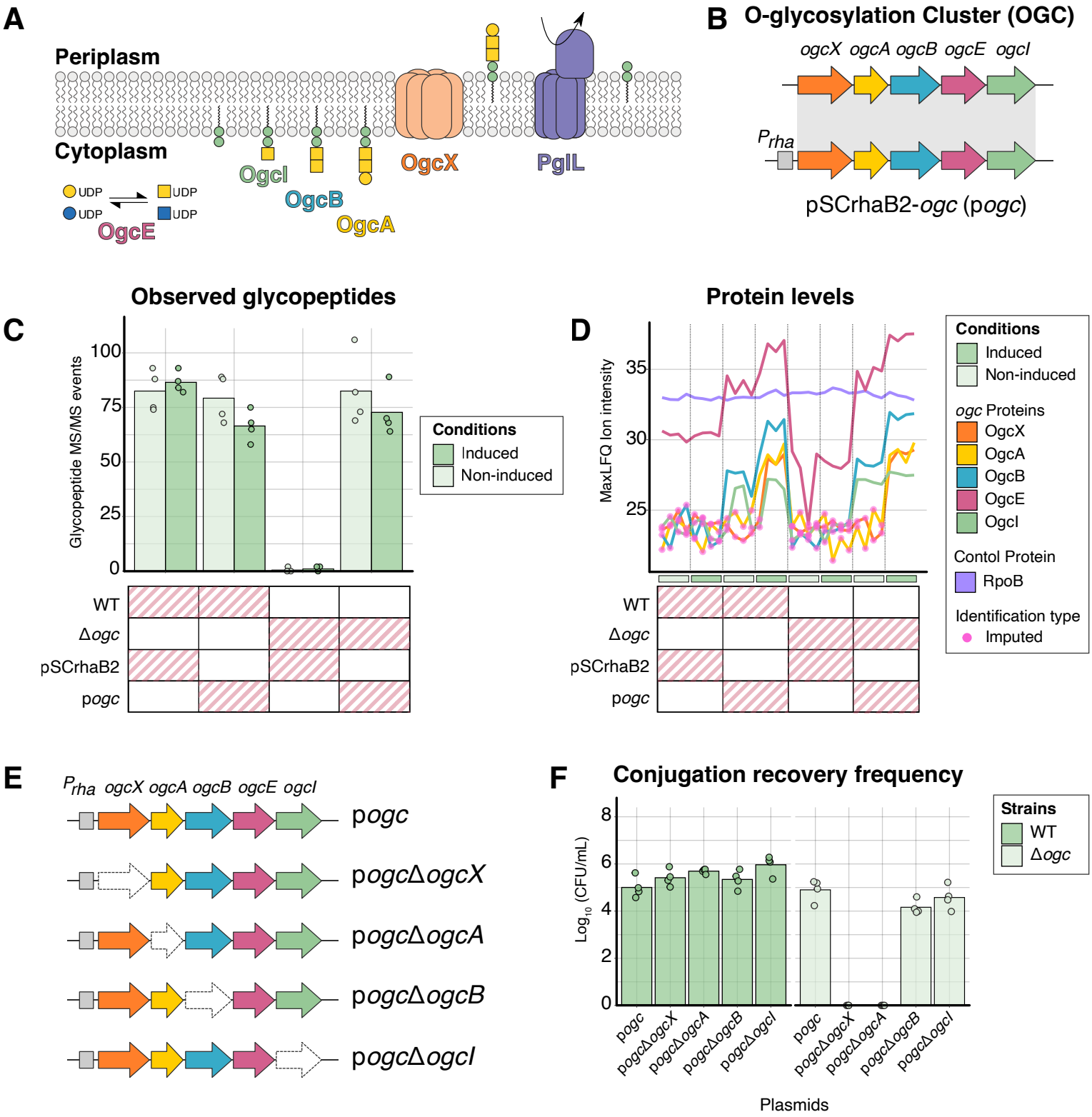
A
Periplasm
Cytoplasm
OgcI
OgcB
OgcA
OgcX
PglL
UDP
UDP
UDP
UDP
OgcE
B
O-glycosylation Cluster (OGC)
ogcX ogcA ogcB ogcE ogcI
Prha
pSCrhaB2-ogc (pogc)
C
Observed glycopeptides
Glycopeptide MS/MS events
100
75
50
25
0
Conditions
Induced
Non-induced
WT
Δogc
pSCrhaB2
pogc
D
Protein levels
MaxLFQ Ion intensity
35
30
25
Conditions
Induced
Non-induced
ogc Proteins
OgcX
OgcA
OgcB
OgcE
OgcI
Contol Protein
RpoB
Identification type
Imputed
WT
Δogc
pSCrhaB2
pogc
E
Prha ogcX ogcA ogcB ogcE ogcI
pogc
pogcΔogcX
pogcΔogcA
pogcΔogcB
pogcΔogcI
F
Conjugation recovery frequency
Log10 (CFU/mL)
8
6
4
2
0
Strains
WT
Δogc
pogc
pogcΔogcX
pogcΔogcA
pogcΔogcB
pogcΔogcI
pogc
pogcΔogcX
pogcΔogcA
pogcΔogcB
pogcΔogcI
Plasmids

Figure 1

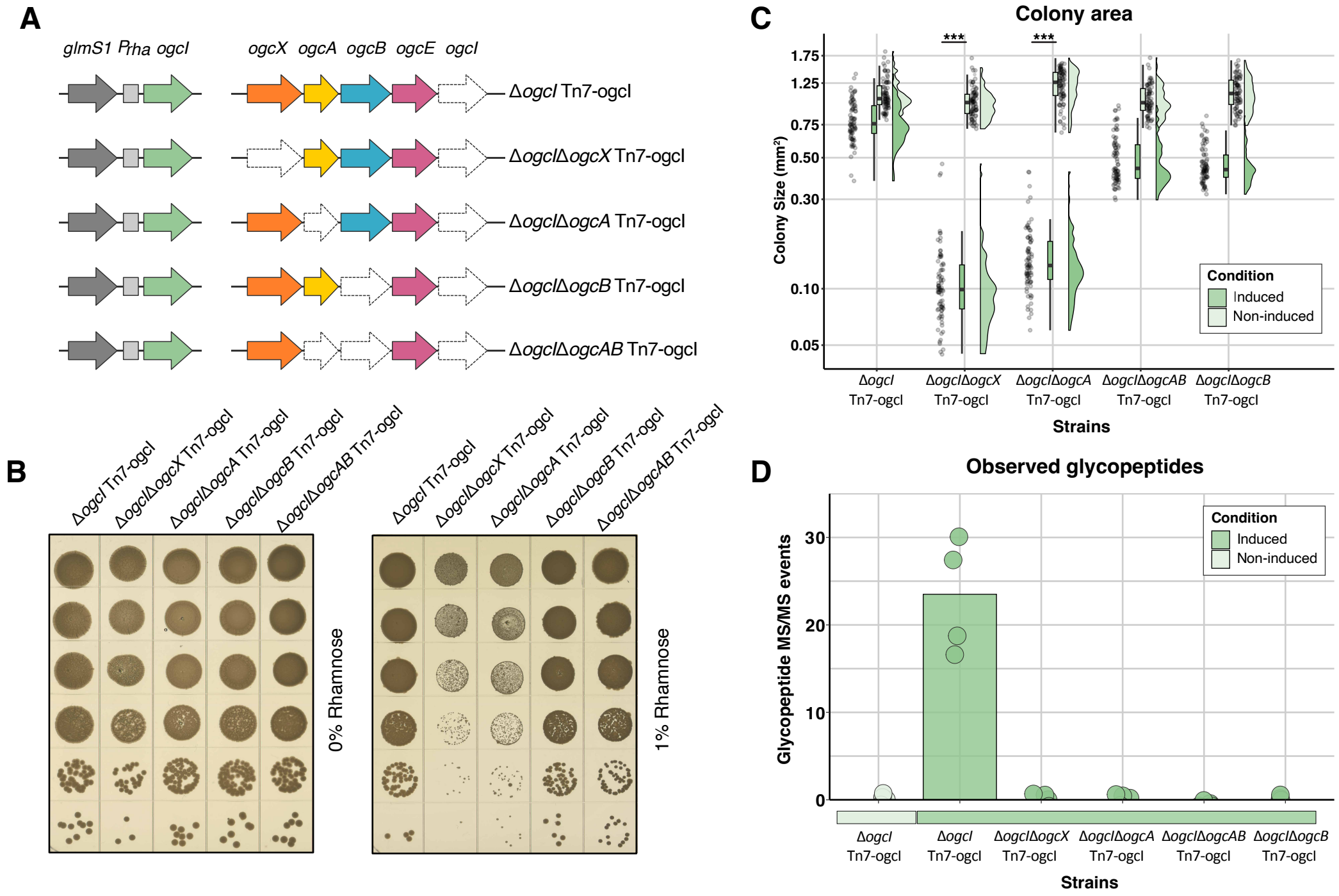
A
glmS1 Prha ogcI
ogcX ogcA ogcB ogcE ogcI
ΔogcI Tn7-ogcI
ΔogcIΔogcX Tn7-ogcI
ΔogcIΔogcA Tn7-ogcI
ΔogcIΔogcB Tn7-ogcI
ΔogcIΔogcAB Tn7-ogcI
B
ΔogcI Tn7-ogcI
ΔogcIΔogcX Tn7-ogcI
ΔogcIΔogcA Tn7-ogcI
ΔogcIΔogcB Tn7-ogcI
ΔogcIΔogcAB Tn7-ogcI
0% Rhamnose
1% Rhamnose
C
Colony area
Colony Size (mm²)
1.75
1.25
0.75
0.50
0.30
0.10
0.05
***
***
Condition
Induced
Non-induced
ΔogcI Tn7-ogcI
ΔogcIΔogcX Tn7-ogcI
ΔogcIΔogcA Tn7-ogcI
ΔogcIΔogcAB Tn7-ogcI
ΔogcIΔogcB Tn7-ogcI
Strains
D
Observed glycopeptides
Glycopeptide MS/MS events
30
20
10
0
Condition
Induced
Non-induced
ΔogcI Tn7-ogcI
ΔogcI Tn7-ogcI
ΔogcIΔogcX Tn7-ogcI
ΔogcIΔogcA Tn7-ogcI
ΔogcIΔogcAB Tn7-ogcI
ΔogcIΔogcB Tn7-ogcI
Strains

Figure 2

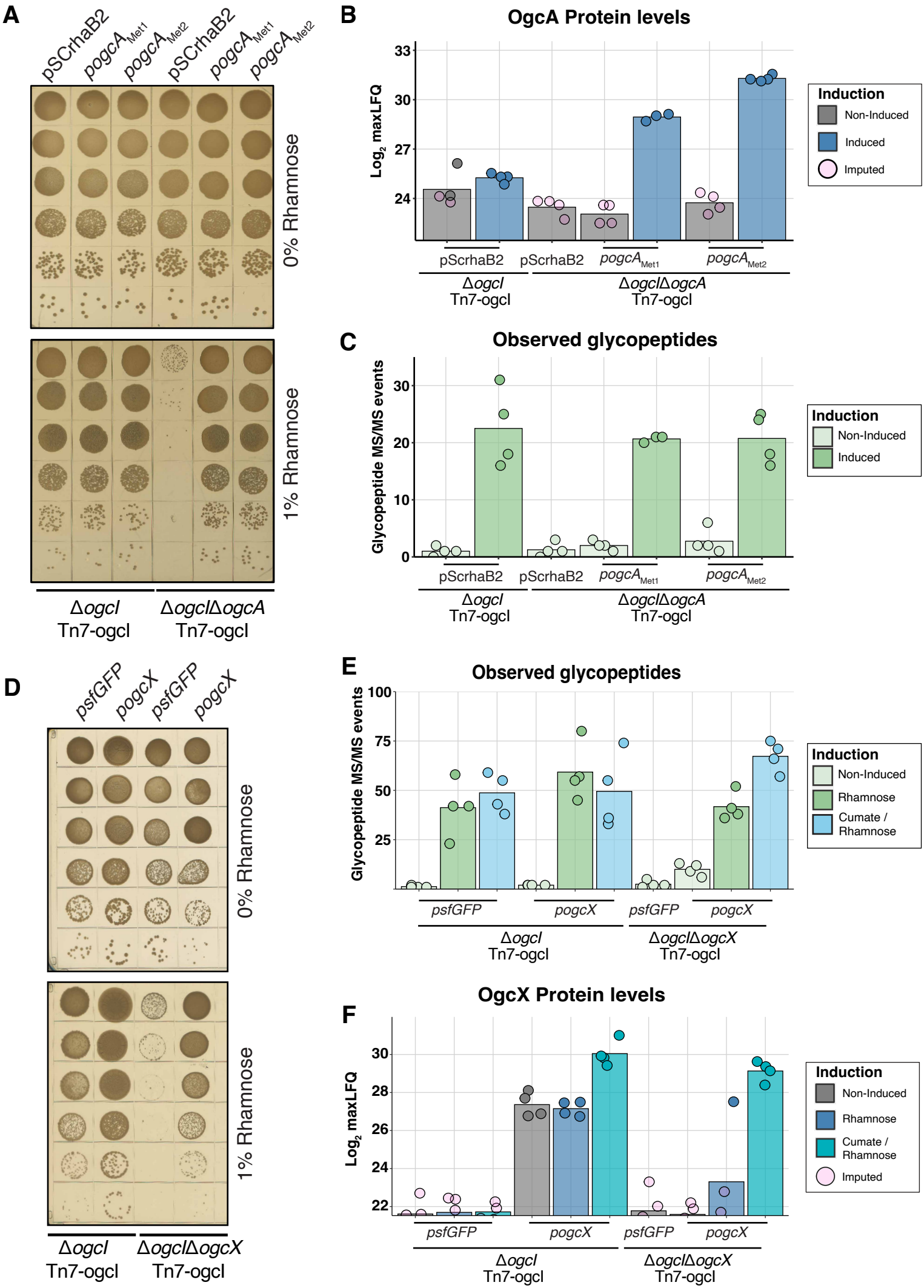
A
pSCrhaB2
pogcA Met1
pogcA Met2
pSCrhaB2
pogcA Met1
pogcA Met2
0% Rhamnose
1% Rhamnose
ΔogcI
Tn7-ogcI
ΔogcIΔogcA
Tn7-ogcI
B
OgcA Protein levels
Log2 maxLFQ
33
30
27
24
pScrhaB2
pScrhaB2
pogcA Met1
pogcA Met2
ΔogcI
Tn7-ogcI
ΔogcIΔogcA
Tn7-ogcI
Induction
Non-Induced
Induced
Imputed
C
Observed glycopeptides
Glycopeptide MS/MS events
30
20
10
0
pScrhaB2
pScrhaB2
pogcA Met1
pogcA Met2
ΔogcI
Tn7-ogcI
ΔogcIΔogcA
Tn7-ogcI
Induction
Non-Induced
Induced
D
psfGFP
pogcX
psfGFP
pogcX
0% Rhamnose
1% Rhamnose
ΔogcI
Tn7-ogcI
ΔogcIΔogcX
Tn7-ogcI
E
Observed glycopeptides
Glycopeptide MS/MS events
100
75
50
25
psfGFP
pogcX
psfGFP
pogcX
ΔogcI
Tn7-ogcI
ΔogcIΔogcX
Tn7-ogcI
Induction
Non-Induced
Rhamnose
Cumate / Rhamnose
F
OgcX Protein levels
Log2 maxLFQ
30
28
26
24
22
psfGFP
pogcX
psfGFP
pogcX
ΔogcI
Tn7-ogcI
ΔogcIΔogcX
Tn7-ogcI
Induction
Non-Induced
Rhamnose
Cumate / Rhamnose
Imputed

Figure 3

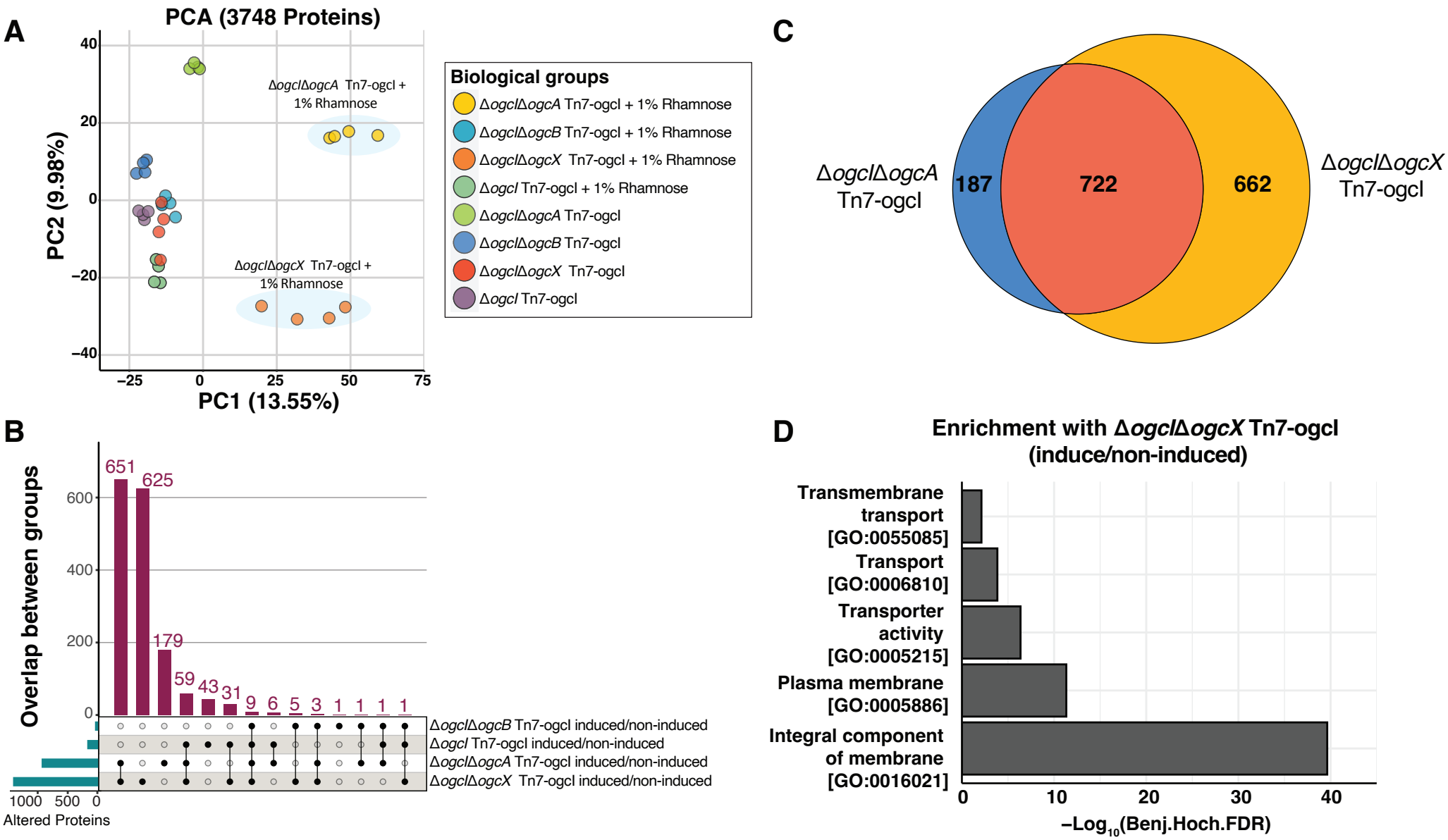
A
PCA (3748 Proteins)
PC2 (9.98%)
PC1 (13.55%)
ΔogclΔogcA Tn7-ogcl + 1% Rhamnose
ΔogclΔogcX Tn7-ogcl + 1% Rhamnose
Biological groups
ΔogclΔogcA Tn7-ogcl + 1% Rhamnose
ΔogclΔogcB Tn7-ogcl + 1% Rhamnose
ΔogclΔogcX Tn7-ogcl + 1% Rhamnose
Δogcl Tn7-ogcl + 1% Rhamnose
ΔogclΔogcA Tn7-ogcl
ΔogclΔogcB Tn7-ogcl
ΔogclΔogcX Tn7-ogcl
Δogcl Tn7-ogcl
B
Overlap between groups
651
625
179
59
43
31
9
6
5
3
1
1
1
1
ΔogclΔogcB Tn7-ogcl induced/non-induced
Δogcl Tn7-ogcl induced/non-induced
ΔogclΔogcA Tn7-ogcl induced/non-induced
ΔogclΔogcX Tn7-ogcl induced/non-induced
Altered Proteins
C
ΔogclΔogcA Tn7-ogcl
187
722
662
ΔogclΔogcX Tn7-ogcl
D
Enrichment with ΔogclΔogcX Tn7-ogcl (induce/non-induced)
Transmembrane transport [GO:0055085]
Transport [GO:0006810]
Transporter activity [GO:0005215]
Plasma membrane [GO:0005886]
Integral component of membrane [GO:0016021]
−Log10(Benj.Hoch.FDR)

Figure 4

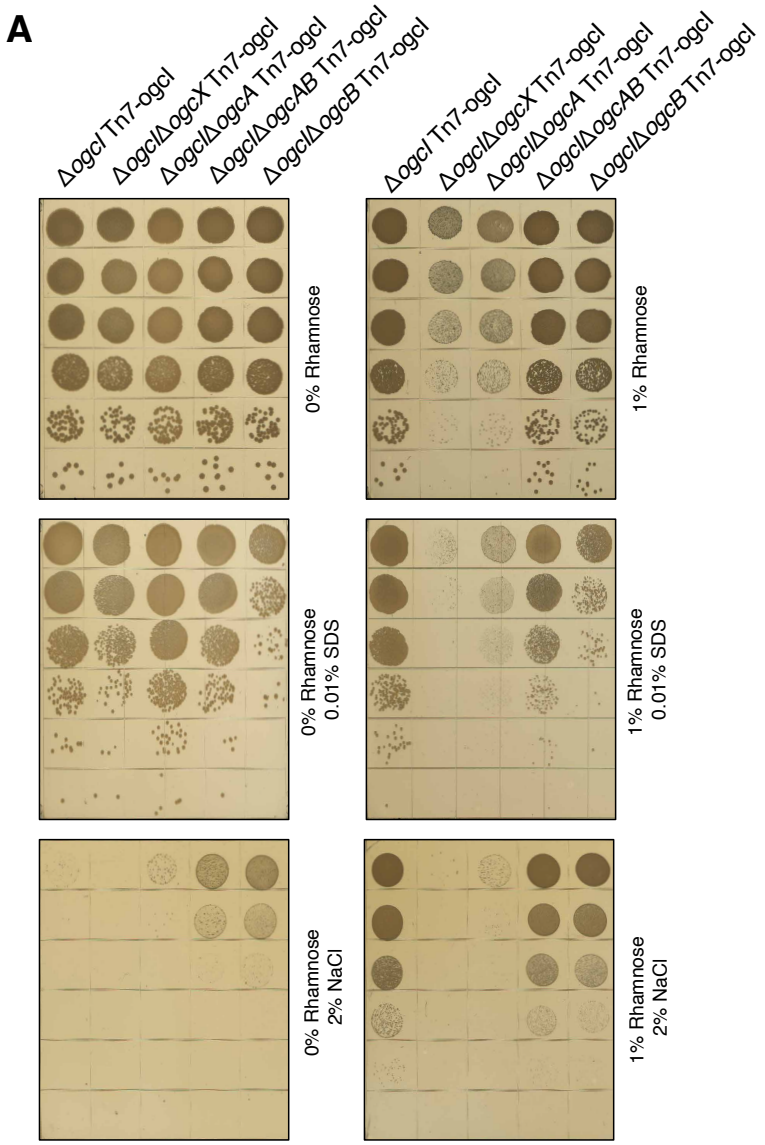
A
ΔogcI Tn7-ogcI
ΔogcIΔogcX Tn7-ogcI
ΔogcIΔogcA Tn7-ogcI
ΔogcIΔogcAB Tn7-ogcI
ΔogcIΔogcB Tn7-ogcI
0% Rhamnose
1% Rhamnose
0% Rhamnose 0.01% SDS
1% Rhamnose 0.01% SDS
0% Rhamnose 2% NaCl
1% Rhamnose 2% NaCl

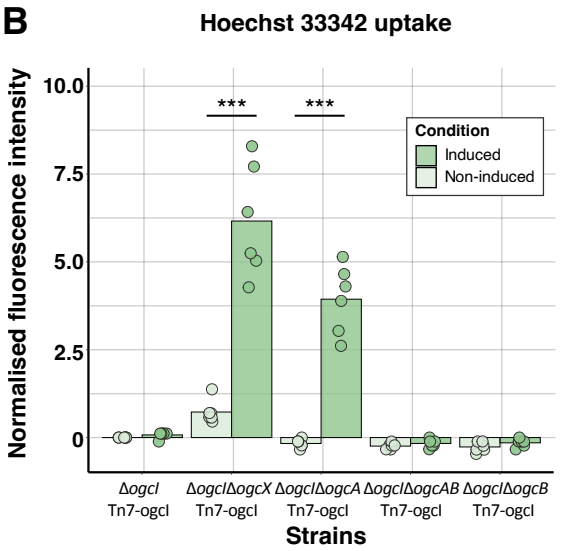
B
Hoechst 33342 uptake
Normalised fluorescence intensity
10.0
7.5
5.0
2.5
0
***
***
Condition
Induced
Non-induced
ΔogcI Tn7-ogcI
ΔogcIΔogcX Tn7-ogcI
ΔogcIΔogcA Tn7-ogcI
ΔogcIΔogcAB Tn7-ogcI
ΔogcIΔogcB Tn7-ogcI
Strains

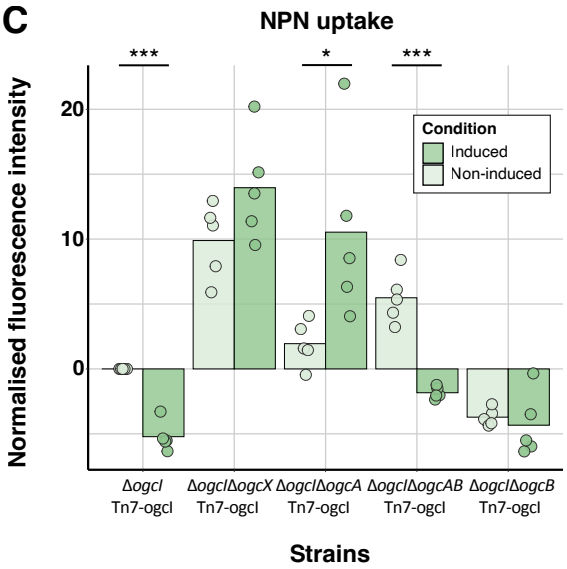
C
NPN uptake
Normalised fluorescence intensity
20
10
0
***
*
***
Condition
Induced
Non-induced
ΔogcI Tn7-ogcI
ΔogcIΔogcX Tn7-ogcI
ΔogcIΔogcA Tn7-ogcI
ΔogcIΔogcAB Tn7-ogcI
ΔogcIΔogcB Tn7-ogcI
Strains

Figure 5

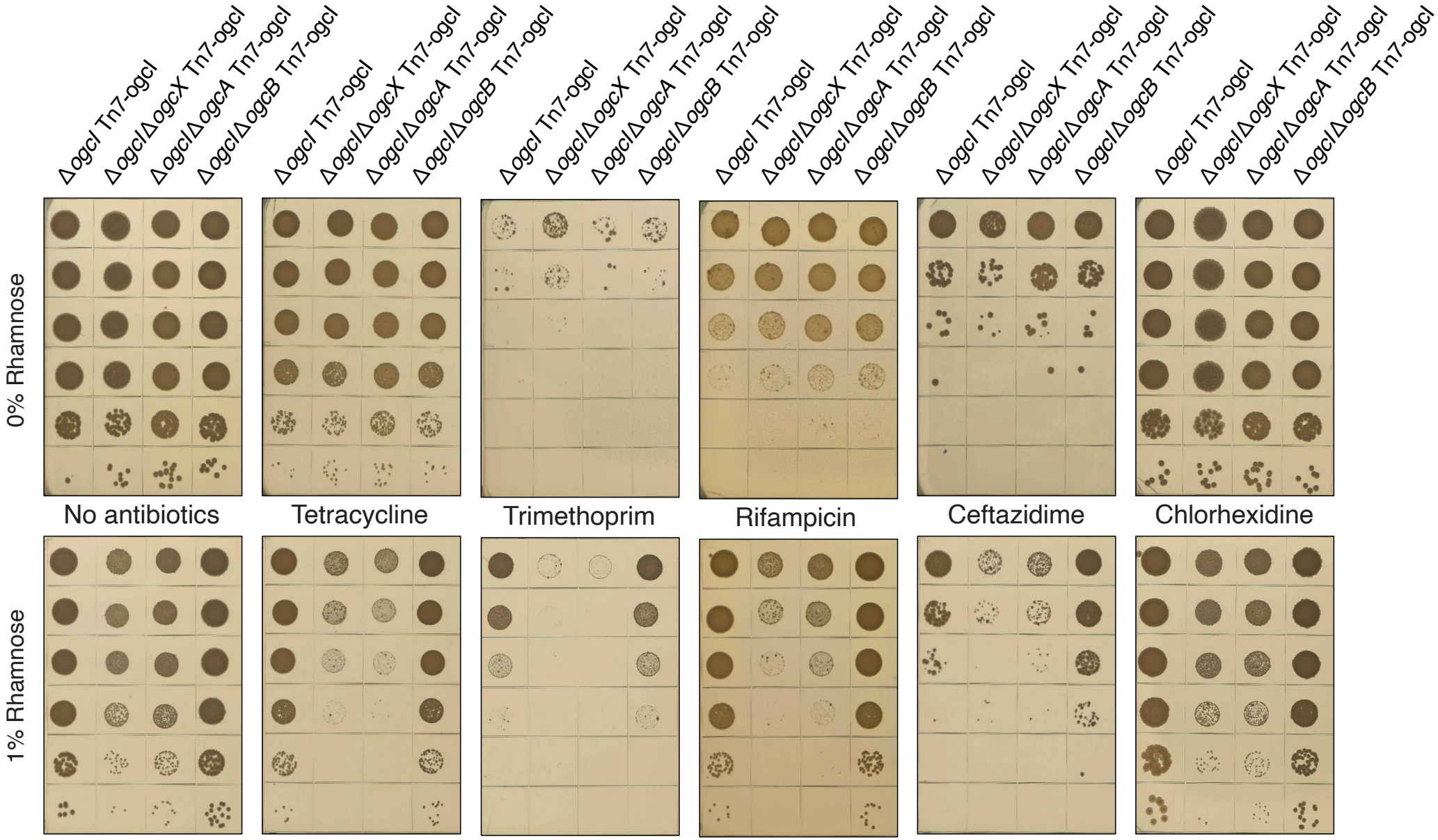
Δogcl Tn7-ogcl
ΔogclΔogcX Tn7-ogcl
ΔogclΔogcA Tn7-ogcl
ΔogclΔogcB Tn7-ogcl
0% Rhamnose
1% Rhamnose
No antibiotics
Tetracycline
Trimethoprim
Rifampicin
Ceftazidime
Chlorhexidine

Figure 6

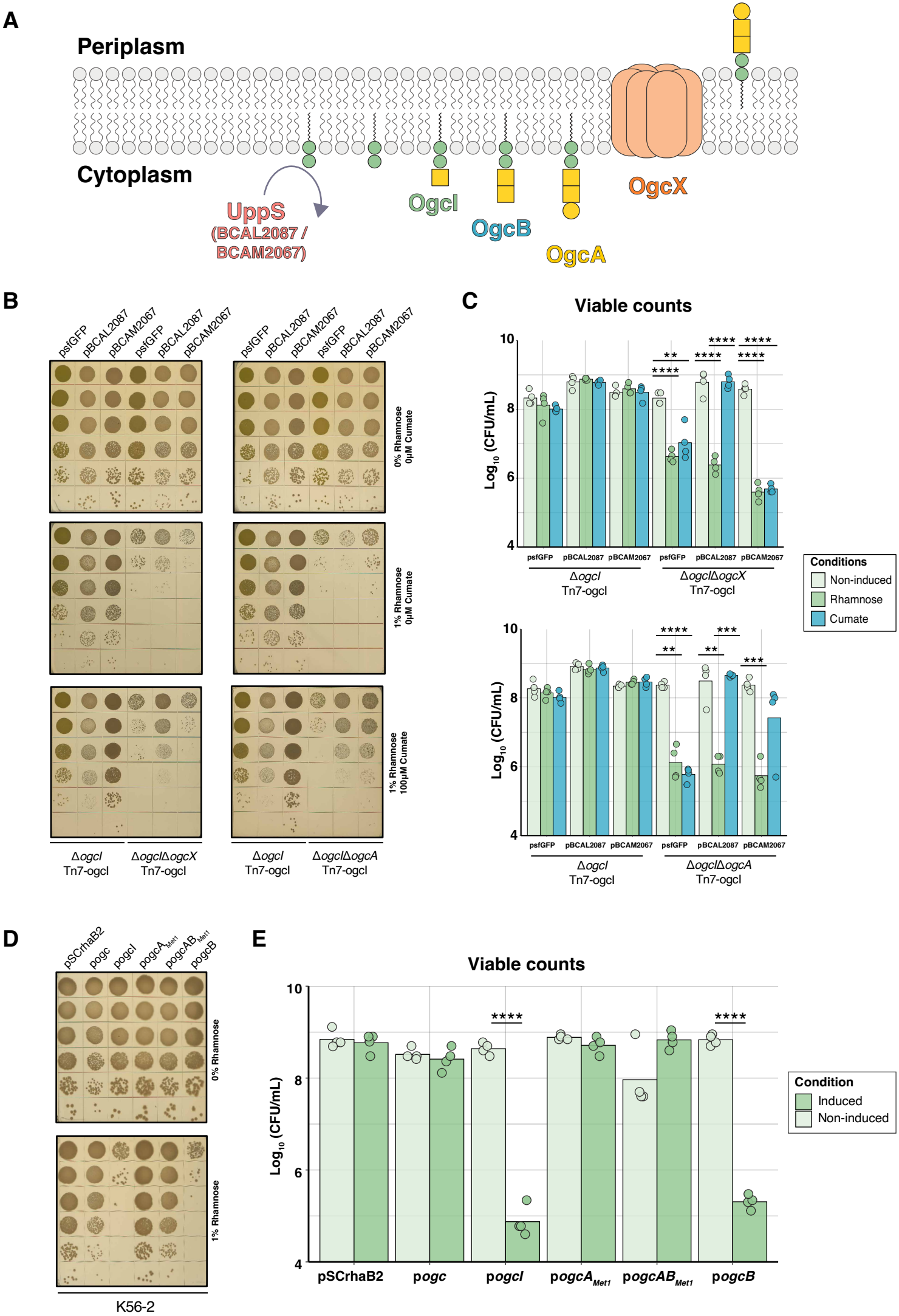
A
Periplasm
Cytoplasm
UppS
(BCAL2087 / BCAM2067)
OgcI
OgcB
OgcA
OgcX
B
psfGFP
pBCAL2087
pBCAM2067
0% Rhamnose 0μM Cumate
1% Rhamnose 0μM Cumate
1% Rhamnose 100μM Cumate
ΔogcI Tn7-ogcI
ΔogcIΔogcX Tn7-ogcI
ΔogcIΔogcA Tn7-ogcI
C
Viable counts
Log10 (CFU/mL)
Conditions
Non-induced
Rhamnose
Cumate
D
pSCrhaB2
pogc
pogcI
pogcAMet1
pogcABMet1
pogcB
0% Rhamnose
1% Rhamnose
K56-2
E
Viable counts
Log10 (CFU/mL)
Condition
Induced
Non-induced
pSCrhaB2
pogc
pogcI
pogcAMet1
pogcABMet1
pogcB

Figure 7